

**Recoil effects in multiphoton electron-positron pair creation**

K. Krajewska\* and J. Z. Kamiński

*Institute of Theoretical Physics, Faculty of Physics, University of Warsaw, Hoża 69, PL-00-681 Warszawa, Poland*

(Received 17 December 2009; published 28 July 2010)

Triply differential probability rates for electron-positron pair creation in laser-nucleus collisions, calculated within the  $S$ -matrix approach, are investigated as functions of the nuclear recoil. Pronounced enhancements of differential probability rates of multiphoton pair production are found for a nonzero momentum transfer from the colliding nucleus. The corresponding rates show a very dramatic dependence on the polarization of the laser field impinging on the nucleus; only for a linearly polarized light are the multiphoton rates for electron-positron pair production considerably large. We focus therefore on this case. Our numerical results for different geometries of the reaction particles demonstrate that, for the linearly polarized laser field of an infinite extent (which is a good approximation for femtosecond laser pulses), the pair creation is far more efficient if the nucleus is detected in the direction of the laser-field propagation. The corresponding angular distributions of the created particles show that the high-energy pairs are predominantly produced in the plane spanned by the polarization vector and the laser-field propagation direction, while the low-energy pairs are rather spread around the latter of the two directions. The enhancement of differential probability rates at each energy sector, defined by the four-momentum conservation relation, is observed with varying the energy of the produced particles. The total probability rates of pair production are also evaluated and compared with the corresponding results for the case when one disregards the recoil effect. A tremendous enhancement of the total probability rates of the electron-positron pair creation is observed if one takes into account the nuclear recoil.

DOI: [10.1103/PhysRevA.82.013420](https://doi.org/10.1103/PhysRevA.82.013420)

PACS number(s): 34.50.Rk, 32.80.Wr, 12.20.Ds

**I. INTRODUCTION**

With the recent development of ultraintense optical lasers, it has become possible to investigate the most fundamental problems of quantum electrodynamics (QED) (see, e.g., Refs. [1–7]), in particular, to probe the structure of the QED vacuum. In this context, we study the electron-positron pair creation in collisions of a highly relativistic nucleus with an ultrastrong electromagnetic plane wave.

Various scenarios of the electron-positron pair production can be found in the literature. Pair creation from the vacuum was analyzed for the first time by Sauter [8] and then reinvestigated by Schwinger [9]. These authors predicted that the pairs can be extracted from the QED vacuum by a static electric field if the respective field strength is at least  $E_{cr} = 1.3 \times 10^{16}$  V/cm. This ruled out the experimental observation of the effect. Later on, the pair creation in an alternating electric field in different regimes (in the nonperturbative, tunneling regime and in the perturbative, high-frequency regime) was treated [10,11]. Again, it turned out that the laser-field strength approaching the critical Schwinger field  $E_{cr}$  is required to observe the process experimentally. With recent developments of very powerful laser sources, in particular the availability of near-visible lasers working currently at intensities  $10^{22}$  W/cm<sup>2</sup> [12,13], and yet more powerful optical lasers built within the European Light Infrastructure project [14], or with the coming x-ray free-electron lasers (XFELs) [15,16], pair production from a vacuum is becoming feasible in the laboratory. Other scenarios of pair creation employ therefore laser pulses which, as long as they are in the femtosecond regime, can be theoretically described by electromagnetic plane waves. One has to remember, however, that the pair production in a

plane-wave field is forbidden by the first principles, as already was noted in [9]. Thus, in the presence of an electromagnetic plane wave, an extra “target” such as a nonlaser photon [17–21], a second counterpropagating field [22–27], or a charged particle [28–46] must be introduced in order to satisfy the energy-momentum conservation law. From the point of view of this article, the latter is of particular importance.

It was Yakovlev who, for the first time, considered the laser-induced electron-positron pair creation in the vicinity of a charged particle [28]. In his article, Yakovlev analyzed the case of a circularly polarized laser wave impinging on a nucleus at rest. This and subsequent works (cf. Refs. [29,40,41]) showed that, for a nucleus at rest, the corresponding cross sections for pair creation are negligibly small. A similar process was analyzed recently taking into account the motion of the target particles; namely, the electron-positron pair creation in laser-heavy-ion collisions was investigated [33–39,42–46]. In all of the aforementioned articles except Ref. [46], the recoil of the target particles was neglected. Most of them also used the standard approach of exactly treating the interaction of the reaction particles with the laser field by means of the so-called Volkov states [47]. In a sense, it is similar therefore to the Keldysh approximation, which is widely used for describing the nonrelativistic multiphoton ionization of atoms and ions [48–51].

The idea of producing electron-positron pairs in laser-nucleus collisions is attributed to Müller *et al.* [33–36], and it originates from the fact that if a nucleus is countermoving with a relativistic velocity (a high Lorentz factor  $\gamma$ ) toward a laser pulse, then in the rest frame of the nucleus the photon frequency is Doppler upshifted by a factor of  $2\gamma$ , as is the peak electric field strength [52]. Thus, for today’s available optical lasers of extreme powers, the peak electric field experienced by the nucleus approaches, in fact, the critical Schwinger value, which is necessary for observing the  $e^-e^+$

\*Katarzyna.Krajewska@fuw.edu.pl

pairs. Let us also mention that the pair creation in collisions of extremely energetic targets with an intense optical laser pulse was realized quite recently at SLAC National Accelerator Laboratory [53,54]. In this experiment, however, an electron beam was involved only indirectly, as it was backscattered by a laser beam to produce  $\gamma$  rays, which in turn collided with the laser beam to produce pairs. Since this indirect mechanism of pair creation turned out to be not very efficient, many efforts have been made since then to describe the direct process [33–39,42–46].

In the works by Müller *et al.* [33–36], the collision of a beam of high energy targets with an extreme-power laser pulse was considered and a circular polarization of the laser pulse was used, since this choice considerably simplifies the treatment of the problem. A general elliptic polarization was also considered in Refs. [35,36], but only for such parameters of the laser field that one observes a few-photon pair production, which relates to the perturbative, high-frequency regime of XFELs. A similar situation was analyzed in Refs. [43–45] for a linearly polarized light. In our contributions so far [37–39,42], we investigated laser-induced pair creation in a linearly polarized laser field and for energies of highly charged ions such that the number of absorbed laser photons was, however, very large (i.e., we worked in the nonperturbative, tunneling regime). Such a situation can be encountered with the use of already available and anticipated optical lasers [12–14]. Our estimates of the total rate for the  $e^-e^+$  pair production (see Ref. [37]), even though still not very big, show, however, that for presently available laser fields the creation of electron-positron pairs by the laser-ion impact process is by far more efficient than the direct creation of pairs from a vacuum through the Schwinger mechanism. In order to improve our theoretical description of the process, leading most likely to improved respective efficiency of the pair production, it is essential now to account for the recoil of target particles.

The most recent work by Müller and Müller [46] is particularly interesting from the point of view of this article as it treats the laser-induced pair production with an exact account of the recoil of colliding nuclei. However, the authors investigate the laser-induced pair creation in the perturbative, high-frequency regime, while the present contribution deals with the nonperturbative, tunneling regime of the process. For this reason, their conclusions cannot be directly related to our case. For instance, while they predict a feasible effect of pair production in the case of a circularly polarized laser field, our calculations for a multiphoton process show a dramatic drop of the probability rates for any polarization of the laser field different than linear; in fact, for a circularly polarized laser pulse, we find negligibly small rates for the multiphoton pair production.

In our case studies, we choose laser-field parameters such that in the reference frame of the colliding nucleus, the frequency and the intensity of the laser field are characterized by numerical values  $\omega = 0.01m_e c^2$  and  $\mu = 100$  [see Eq. (8)]. For heavy nuclei, such parameters are rather hardly to be met in the present-day lasers and ion-accelerators. However, these conditions can be fulfilled if one combines already-operating lasers [13] with proton (Large Hadron Collider) or electron (Large Electron-Positron Collider and TESLA) accelerators. In this context, it seems to be of a great importance to construct a tabletop laser source of extreme power. Such efforts are being

made [55], which would make it even more realistic to observe the laser-induced pair production in the tunneling regime.

In this contribution, we focus our attention mainly on the theoretical methods and on the general characteristics of the electron-positron pair-creation process in heavy-nuclei collisions with very strong laser fields. Emphasis is placed on the similarities and differences between this process and its related phenomenon—the multiphoton (called also above-threshold) ionization of atoms or ions in nonrelativistic quantum mechanics. Analysis of pair-creation process for intense laser-field parameters achievable now or in the near future [12–14,55] and for energies of charged particles (such as heavy nuclei, protons, or electrons) in contemporary accelerators will be presented elsewhere.

This article is organized as follows. In Sec. II, we present general solutions of the Dirac equation for both a particle and an antiparticle in an electromagnetic plane-wave field of an elliptic polarization. Then, the derivations of the  $S$ -matrix amplitude for electron-positron pair creation in the laser-nucleus impact process in the first-order Born approximation and the probability rates for a particular number  $N$  of absorbed laser photons are outlined. Numerical results are presented in Secs. III and IV. In particular, in Sec. III, we demonstrate the dependence of differential probability rates for the  $e^-e^+$  pair production on the nuclear recoil in the case of an equal energy sharing between the produced particles. The dependence on the polarization of the laser field also is analyzed. The more general situation, that is, when the created particles have different energies, still allowed by the energy-momentum conservation principle, is investigated in Sec. IV. The way of solving this conservation law is presented in the Appendix. For a reason that becomes clear later on, in Sec. IV, we only consider the case of a linearly polarized light. In Sec. IV, the main focus is on angular distributions of created particles, which makes it possible to predict the geometry in which pairs are predominantly created. In Sec. V, the total probability rates for the electron-positron pair creation using the Monte Carlo method are calculated. Comparison with the related results obtained for the case when one disregards the nuclear recoil is also demonstrated. The final section, Sec. VI, is devoted to a summary of our results and to some concluding remarks.

## II. THEORY

In the theoretical part, we employ the units in which  $\hbar = 1$ . However, in our numerical analysis which follows we take also  $c = 1$  and  $m_e = 1$ , where  $m_e$  is the electron mass; that is, we use the relativistic units. Furthermore, we denote the product of any two four-vectors  $a^\mu$  and  $b^\mu$  with  $a \cdot b = a_\mu b^\mu$  ( $\mu = 0, 1, 2, 3$ ), where the Einstein summation convention is used. We employ the Feynman notation  $\not{a} = \gamma \cdot a = \gamma^\mu a_\mu$  for the contraction with the Dirac  $\gamma$  matrices  $\gamma^\mu$ . Finally, we use a customary notation  $\bar{a} = a^\dagger \gamma^0$ , where  $a^\dagger$  is the Hermitian conjugate of  $a$ .

### A. Volkov waves

In the present work, we consider an electromagnetic plane-wave field propagating along a unit vector  $\mathbf{n}$  that is represented by the four-vector potential  $A^\mu = A^\mu(k \cdot x)$ ,

where  $k \cdot x$  is expressed in terms of the wave four-vector  $k = (\omega/c)(1, \mathbf{n})$ , with  $\omega$  being the angular frequency of the laser-field oscillations. Since  $k \cdot A = 0$  and  $k^2 = 0$ , one derives the exact relativistic solutions of the Dirac equation coupled to the electromagnetic plane-wave field; these solutions are known in the literature as the Volkov waves [47].

We consider here a particle of mass  $m$  and charge  $\mathcal{Z}e$  (where  $e$  is the electron charge,  $e < 0$ , and  $\mathcal{Z}$  can be either positive or negative and is related to the atomic number  $Z$  such that  $|\mathcal{Z}| = Z$ ), for which the Volkov wave  $\psi_{p,\lambda}^{(\pm)}(x)$  fulfills the equation

$$(i\partial - \mathcal{Z}eA - mc)\psi_{p,\lambda}^{(\pm)}(x) = 0. \quad (1)$$

Here, the indices  $p$  and  $\lambda$  refer to the particle momentum outside the laser focus and to its spin projection, respectively, while the indices  $(\pm)$  label positive- and negative-energy quantum states that describe either a particle (+) or an antiparticle (-). The Volkov solutions, normalized in the volume  $V$ , have the general form

$$\psi_{p,\lambda}^{(\pm)}(x) = \sqrt{\frac{mc^2}{VE_p}} \left( 1 \mp \frac{\mathcal{Z}e}{2k \cdot p} A k \right) u_{p,\lambda}^{(\pm)} e^{\mp i S_p^{(\pm)}(x)}, \quad (2)$$

where  $u_{p,\lambda}^{(\pm)}$  are four-spinors satisfying the field-free equations,  $(\not{p} \mp mc)u_{p,\lambda}^{(\pm)} = 0$ , with the same convention regarding the indices  $(\pm)$  as before (see also Ref. [56]), while the phase

$$S_p^{(\pm)} = p \cdot x + \int^{k \cdot x} \left( \pm \mathcal{Z}e \frac{A(\phi) \cdot p}{k \cdot p} - (\mathcal{Z}e)^2 \frac{A^2(\phi)}{2k \cdot p} \right) d\phi \quad (3)$$

has a meaning of the classical action of a charged particle (antiparticle) in the laser field.

In the most general case when a monochromatic, elliptically polarized plane wave with two unit four-vectors  $\varepsilon_1$  and  $\varepsilon_2$  and an angle  $\delta$ , describing the ellipticity, are used, the four-vector potential is given by

$$A^\mu(k \cdot x) = A_0 [\varepsilon_1^\mu \cos \delta \cos(k \cdot x) + \varepsilon_2^\mu \sin \delta \sin(k \cdot x)]. \quad (4)$$

Here,  $A_0$  is the amplitude of the vector potential, while the polarization four-vectors are  $\varepsilon_i = (0, \mathbf{e}_i)$ , with  $i = 1, 2$ ,

$$\varepsilon_1^2 = \varepsilon_2^2 = -\mathbf{e}_1^2 = -\mathbf{e}_2^2 = -1, \quad \varepsilon_1 \cdot \varepsilon_2 = -\mathbf{e}_1 \cdot \mathbf{e}_2 = 0. \quad (5)$$

In this case, the classical action  $S_p^{(\pm)}$ , as defined by Eq. (3), can be written in the form

$$S_p^{(\pm)}(x) = \bar{p} \cdot x + Q_p^{(\pm)}(k \cdot x), \quad (6)$$

where we introduce the so-called dressed four-momentum of a particle in the laser field,

$$\bar{p} = p + \frac{(\mathcal{Z}eA_0)^2}{4k \cdot p} k, \quad (7)$$

satisfying the effective-mass on-shell relation  $\bar{p}^2 = (\bar{m}c)^2$ . Here the effective mass  $\bar{m}$  equals  $\bar{m}^2 = m^2 + \mathcal{Z}^2 \mu^2 m_e^2 / 2$ , where  $\mu$  is the dimensionless and relativistically invariant parameter that is related to the amplitude  $A_0$  of the laser

field,

$$\mu = \frac{|eA_0|}{m_e c}. \quad (8)$$

At this point let us also remind the reader that the bare momentum  $p$ , which is defined outside the laser focus, is on the mass shell,  $p^2 = (mc)^2$ . Going back to Eqs. (3) and (6), we conclude that in the present case of an elliptically polarized light, the phase  $Q_p^{(\pm)}(k \cdot x)$  equals

$$\begin{aligned} Q_p^{(\pm)}(k \cdot x) = & \pm \mathcal{Z}eA_0 \frac{\varepsilon_1 \cdot p}{k \cdot p} \cos \delta \sin(k \cdot x) \\ & \mp \mathcal{Z}eA_0 \frac{\varepsilon_2 \cdot p}{k \cdot p} \sin \delta \cos(k \cdot x) \\ & + \frac{(\mathcal{Z}eA_0)^2}{8k \cdot p} \cos(2\delta) \sin(2k \cdot x), \end{aligned} \quad (9)$$

which is a periodic function of its argument  $k \cdot x$ , and so will lead later on to the Fourier expansion of the  $S$ -matrix element.

## B. $S$ -matrix transition amplitude

The process of electron-positron pair creation in laser-nucleus collisions, represented graphically by the diagram in Fig. 1, can be described within the  $S$ -matrix formalism. The relevant transition amplitude is given by

$$\begin{aligned} S_{fi} = & -4\pi i \mathcal{Z} \alpha \int d^4x \int d^4y j_{p_e^- p_e^+}^\mu(x) \\ & \times \mathcal{D}_{\mu\nu}(x-y) j_{q_i q_f}^\nu(y), \end{aligned} \quad (10)$$

where the fine-structure constant is  $\alpha = e^2/(4\pi\epsilon_0 c)$ . Here  $(p_e^-, p_e^+)$  are the bare four-momenta of the created electron and positron, while  $(q_i, q_f)$  are the bare incoming and outgoing four-momenta of a nucleus. Further,  $j_{p_e^- p_e^+}^\mu(x)$  and  $j_{q_i q_f}^\nu(y)$  denote the relativistic four-currents of a pair and a nucleus, respectively,

$$j_{p_e^- p_e^+}^\mu(x) = \bar{\psi}_{p_e^- \lambda_e^-}^{(+)}(x) \gamma^\mu \psi_{p_e^+ \lambda_e^+}^{(-)}(x), \quad (11)$$

$$j_{q_i q_f}^\nu(y) = \bar{\psi}_{q_i \lambda_i}^{(+)}(y) \gamma^\nu \psi_{q_f \lambda_f}^{(+)}(y), \quad (12)$$

where the Volkov solutions (2) with appropriate  $m$  and  $\mathcal{Z}$  [ $m = m_e$  and  $\mathcal{Z} = 1$  in Eq. (11), or  $m = M_N$  and  $\mathcal{Z} < 0$  in Eq. (12), where  $M_N$  is the nucleus mass] should be substituted.

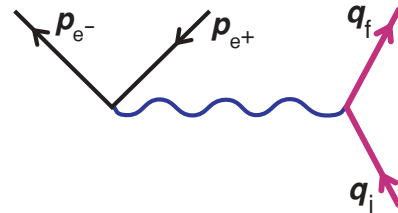


FIG. 1. (Color online) Feynman diagram for electron-positron pair creation during the laser-nucleus collision in the lowest order of approximation with respect to the radiative corrections (the so-called tree approximation). Each spin-1/2 particle, which includes also the nucleus, is described by the corresponding Volkov wave for a Dirac particle in an electromagnetic plane-wave field of an arbitrary strength.

The photon propagator  $\mathcal{D}_{\mu\nu}(x-y)$ , which appears in Eq. (10), is given by

$$\mathcal{D}_{\mu\nu}(x-y) = \int \frac{d^4\mathcal{K}}{(2\pi)^4} \tilde{\mathcal{D}}_{\mu\nu}(\mathcal{K}) e^{-i\mathcal{K}\cdot(x-y)}, \quad (13)$$

$$\tilde{\mathcal{D}}_{\mu\nu}(\mathcal{K}) = -\frac{1}{\mathcal{K}^2} \left( g_{\mu\nu} - \xi_G \frac{\mathcal{K}_\mu \mathcal{K}_\nu}{\mathcal{K}^2} \right), \quad (14)$$

with  $\xi_G$  being the gauge-fixing constant. Taking into account that currents (11) and (12) satisfy the conservation law,  $\partial_\mu j^\mu = 0$ , we conclude that the  $S$ -matrix element does not depend on  $\xi_G$  and so it is gauge invariant. For this reason, the gauge-dependent part of the photon propagator can be neglected (we put, therefore,  $\xi_G = 0$ ).

Now, let us present the four-currents (11) and (12) in a more explicit form. Substituting the Volkov solutions (2) into Eqs. (11) and (12), we obtain

$$\begin{aligned} j_{p_e^- p_e^+}^\mu(x) &= \frac{m_e c^2}{V \sqrt{E_{p_e^-} E_{p_e^+}}} \bar{u}_{p_e^- \lambda_e^-}^{(+)} \left( 1 + \frac{eA\mathcal{k}}{2k \cdot p_e^-} \right) \\ &\times \gamma^\mu \left( 1 + \frac{eA\mathcal{k}}{2k \cdot p_e^+} \right) u_{p_e^+ \lambda_e^+}^{(-)} e^{i(\bar{p}_e^- + \bar{p}_e^+) \cdot x} \\ &\times e^{iQ_{p_e^-}(k \cdot x) + iQ_{p_e^+}(k \cdot x)}, \end{aligned} \quad (15)$$

and similarly,

$$\begin{aligned} j_{q_f q_i}^\nu(y) &= \frac{M_N c^2}{V \sqrt{E_{q_f} E_{q_i}}} \bar{u}_{q_i \lambda_i}^{(+)} \left( 1 + \frac{ZeA\mathcal{k}}{2k \cdot q_f} \right) \gamma^\nu \left( 1 - \frac{ZeA\mathcal{k}}{2k \cdot q_i} \right) \\ &\times u_{q_f \lambda_f}^{(+)} e^{i(\bar{q}_f - \bar{q}_i) \cdot y} e^{iQ_{q_f}(k \cdot y) - iQ_{q_i}(k \cdot y)}, \end{aligned} \quad (16)$$

where the relation (6) has been used. Since both currents are periodic functions of  $k \cdot x$  and  $k \cdot y$ , respectively, we can represent them as a Fourier series each. Doing so, we arrive at the following decompositions:

$$\begin{aligned} j_{p_e^- p_e^+}^\mu(x) &= \frac{m_e c^2}{V \sqrt{E_{p_e^-} E_{p_e^+}}} \sum_{N=-\infty}^{\infty} e^{-i(Nk - \bar{p}_e^- - \bar{p}_e^+) \cdot x} \\ &\times \mathcal{C}_N^\mu(p_e^- \lambda_e^-, p_e^+ \lambda_e^+), \end{aligned} \quad (17)$$

$$\begin{aligned} j_{q_f q_i}^\nu(y) &= \frac{M_N c^2}{V \sqrt{E_{q_f} E_{q_i}}} \sum_{N=-\infty}^{\infty} e^{-i(Nk + \bar{q}_i - \bar{q}_f) \cdot y} \\ &\times \mathcal{F}_N^\nu(q_f \lambda_f, q_i \lambda_i), \end{aligned} \quad (18)$$

which define the Fourier coefficients  $\mathcal{C}_N^\mu(p_e^- \lambda_e^-, p_e^+ \lambda_e^+)$  and  $\mathcal{F}_N^\nu(q_f \lambda_f, q_i \lambda_i)$ . One can show that these coefficients can be expressed in terms of the generalized Bessel function  $B_N$ , which is an infinite sum over products of ordinary Bessel functions  $J_N$  such that

$$B_N(x, y, \theta) = \sum_{N'=-\infty}^{\infty} J_{N-2N'}(x) J_{N'}(y) e^{-iN'\theta}. \quad (19)$$

Noting that in the case considered in this article, the function  $e^{iQ_{p_e^-}(k \cdot x) + iQ_{p_e^+}(k \cdot x)}$  in Eq. (15) can be rewritten as  $e^{-ia \sin(k \cdot x + \eta) - ib \sin(2k \cdot x)}$ , where the coefficients  $a, b, \eta$  follow from Eq. (9), we find out that

$$e^{iQ_{p_e^-}(k \cdot x) + iQ_{p_e^+}(k \cdot x)} = \sum_{N=-\infty}^{\infty} e^{-iN(k \cdot x + \eta)} B_N(a, b, -2\eta), \quad (20)$$

with

$$\begin{aligned} eA_0 \left( \frac{\varepsilon_1 \cdot p_e^-}{k \cdot p_e^-} - \frac{\varepsilon_1 \cdot p_e^+}{k \cdot p_e^+} \right) \cos \delta &= -a \cos \eta, \\ eA_0 \left( \frac{\varepsilon_2 \cdot p_e^-}{k \cdot p_e^-} - \frac{\varepsilon_2 \cdot p_e^+}{k \cdot p_e^+} \right) \sin \delta &= a \sin \eta, \\ \frac{(eA_0)^2}{8} \left( \frac{1}{k \cdot p_e^-} + \frac{1}{k \cdot p_e^+} \right) \cos(2\delta) &= -b. \end{aligned} \quad (21)$$

Since the same applies to the function  $e^{iQ_{q_f}(k \cdot y) - iQ_{q_i}(k \cdot y)}$ , we have also

$$e^{iQ_{q_f}(k \cdot y) - iQ_{q_i}(k \cdot y)} = \sum_{N=-\infty}^{\infty} e^{-iN(k \cdot y + \xi)} B_N(u, v, -2\xi), \quad (22)$$

where

$$\begin{aligned} ZeA_0 \left( \frac{\varepsilon_1 \cdot q_f}{k \cdot q_f} - \frac{\varepsilon_1 \cdot q_i}{k \cdot q_i} \right) \cos \delta &= -u \cos \xi, \\ ZeA_0 \left( \frac{\varepsilon_2 \cdot q_f}{k \cdot q_f} - \frac{\varepsilon_2 \cdot q_i}{k \cdot q_i} \right) \sin \delta &= u \sin \xi, \\ \frac{(ZeA_0)^2}{8} \left( \frac{1}{k \cdot q_f} - \frac{1}{k \cdot q_i} \right) \cos(2\delta) &= -v. \end{aligned} \quad (23)$$

The Fourier decomposition of the four-currents into the generalized Bessel functions and finding the related coefficients  $\mathcal{C}_N^\mu$  and  $\mathcal{F}_N^\nu$  seem to be straightforward now. Hence, let us present the final formulas for  $\mathcal{C}_N^\mu$  and  $\mathcal{F}_N^\nu$ :

$$\begin{aligned} \mathcal{C}_N^\mu(p_e^- \lambda_e^-, p_e^+ \lambda_e^+) &= e^{-iN\eta} \bar{u}_{p_e^- \lambda_e^-}^{(+)} \left[ \gamma^\mu B_N(a, b, -2\eta) + \frac{eA_0}{4} \cos \delta \left( \frac{\not{\varepsilon}_1 \not{k} \gamma^\mu}{k \cdot p_e^-} + \frac{\gamma^\mu \not{\varepsilon}_1 \not{k}}{k \cdot p_e^+} \right) [e^{-i\eta} B_{N+1}(a, b, -2\eta) \right. \right. \\ &+ e^{i\eta} B_{N-1}(a, b, -2\eta)] + \frac{eA_0}{4i} \sin \delta \left( \frac{\not{\varepsilon}_2 \not{k} \gamma^\mu}{k \cdot p_e^-} + \frac{\gamma^\mu \not{\varepsilon}_2 \not{k}}{k \cdot p_e^+} \right) [e^{-i\eta} B_{N+1}(a, b, -2\eta) - e^{i\eta} B_{N-1}(a, b, -2\eta)] \\ &+ \frac{(eA_0)^2 \cos^2 \delta}{16(k \cdot p_e^-)(k \cdot p_e^+)} \not{\varepsilon}_1 \not{k} \gamma^\mu \not{\varepsilon}_1 \not{k} [e^{-2i\eta} B_{N+2}(a, b, -2\eta) + 2B_N(a, b, -2\eta) + e^{2i\eta} B_{N-2}(a, b, -2\eta)] \\ &- \frac{(eA_0)^2 \sin^2 \delta}{16(k \cdot p_e^-)(k \cdot p_e^+)} \not{\varepsilon}_2 \not{k} \gamma^\mu \not{\varepsilon}_2 \not{k} [e^{-2i\eta} B_{N+2}(a, b, -2\eta) - 2B_N(a, b, -2\eta) + e^{2i\eta} B_{N-2}(a, b, -2\eta)] \\ &+ \left. \frac{(eA_0)^2 \sin 2\delta}{32i(k \cdot p_e^-)(k \cdot p_e^+)} (\not{\varepsilon}_1 \not{k} \gamma^\mu \not{\varepsilon}_2 \not{k} + \not{\varepsilon}_2 \not{k} \gamma^\mu \not{\varepsilon}_1 \not{k}) [e^{-2i\eta} B_{N+2}(a, b, -2\eta) - e^{2i\eta} B_{N-2}(a, b, -2\eta)] \right] u_{p_e^+ \lambda_e^+}^{(-)} \end{aligned} \quad (24)$$

and

$$\begin{aligned}
 \mathcal{F}_N^v(q_f \lambda_f, q_i \lambda_i) = & e^{-iN\xi} \bar{u}_{q_f \lambda_f}^{(+)} \left[ \gamma^\nu B_N(u, v, -2\xi) + \frac{ZeA_0}{4} \cos \delta \left( \frac{\not{\epsilon}_1 \not{k} \gamma^\nu}{k \cdot q_f} - \frac{\gamma^\nu \not{\epsilon}_1 \not{k}}{k \cdot q_i} \right) [e^{-i\xi} B_{N+1}(u, v, -2\xi) \right. \\
 & + e^{i\xi} B_{N-1}(u, v, -2\xi)] + \frac{ZeA_0}{4i} \sin \delta \left( \frac{\not{\epsilon}_2 \not{k} \gamma^\nu}{k \cdot q_f} - \frac{\gamma^\nu \not{\epsilon}_2 \not{k}}{k \cdot q_i} \right) [e^{-i\xi} B_{N+1}(u, v, -2\xi) - e^{i\xi} B_{N-1}(u, v, -2\xi)] \\
 & - \frac{(ZeA_0)^2 \cos^2 \delta}{16(k \cdot q_f)(k \cdot q_i)} \not{\epsilon}_1 \not{k} \gamma^\nu \not{\epsilon}_1 \not{k} [e^{-2i\xi} B_{N+2}(u, v, -2\xi) + 2B_N(u, v, -2\xi) + e^{2i\xi} B_{N-2}(u, v, -2\xi)] \\
 & + \frac{(ZeA_0)^2 \sin^2 \delta}{16(k \cdot q_f)(k \cdot q_i)} \not{\epsilon}_2 \not{k} \gamma^\nu \not{\epsilon}_2 \not{k} [e^{-2i\xi} B_{N+2}(u, v, -2\xi) - 2B_N(u, v, -2\xi) + e^{2i\xi} B_{N-2}(u, v, -2\xi)] \\
 & \left. - \frac{(ZeA_0)^2 \sin 2\delta}{32i(k \cdot q_f)(k \cdot q_i)} (\not{\epsilon}_1 \not{k} \gamma^\nu \not{\epsilon}_2 \not{k} + \not{\epsilon}_2 \not{k} \gamma^\nu \not{\epsilon}_1 \not{k}) [e^{-2i\xi} B_{N+2}(u, v, -2\xi) - e^{2i\xi} B_{N-2}(u, v, -2\xi)] \right] u_{q_i \lambda_i}^{(+)} \quad (25)
 \end{aligned}$$

Introducing expressions (13), (17), and (18) into Eq. (10) and performing the relevant space-time integrals exactly, we arrive at

$$\begin{aligned}
 S_{\text{fi}} = & \frac{-4\pi i Z\alpha}{\sqrt{E_{q_f} E_{q_i} E_{p_e^-} E_{p_e^+}}} \frac{m_e M_N c^4}{V^2} (2\pi)^4 \sum_{M,L} \int d^4 K \\
 & \times \delta(Mk + K - \bar{p}_{e^-} - \bar{p}_{e^+}) \delta(Lk - K + \bar{q}_i - \bar{q}_f) \\
 & \times C_M^\mu(p_{e^-} \lambda_{e^-}, p_{e^+} \lambda_{e^+}) \tilde{D}_{\mu\nu}(K) \mathcal{F}_L^v(q_f \lambda_f, q_i \lambda_i). \quad (26)
 \end{aligned}$$

Even though the laser field is treated classically, one concludes from this equation that numbers  $M$  and  $L$  can be interpreted as numbers of photons that are either absorbed from or emitted into the laser field by the pair ( $M$ ) or by the nucleus ( $L$ ). Let then  $N$  be the total number of photons that are exchanged with the field,  $N = M + L$ . Thus, we find from Eq. (26)

$$\begin{aligned}
 S_{\text{fi}} = & \sum_N S_{\text{fi}}^{(N)} \delta(\bar{q}_i - \bar{q}_f - \bar{p}_{e^-} - \bar{p}_{e^+} + Nk) \\
 = & -4\pi i Z\alpha (2\pi)^4 \sum_N \delta(\bar{q}_i - \bar{q}_f - \bar{p}_{e^-} - \bar{p}_{e^+} + Nk) \\
 & \times \frac{m_e M_N c^4}{V^2} \frac{t_N(p_{e^-} \lambda_{e^-}, p_{e^+} \lambda_{e^+}; q_f \lambda_f, q_i \lambda_i)}{\sqrt{E_{q_f} E_{q_i} E_{p_e^-} E_{p_e^+}}}, \quad (27)
 \end{aligned}$$

where the first row in this equation implicitly defines the  $N$ th order  $S$ -matrix element,  $S_{\text{fi}}^{(N)}$ , while the argument of the  $\delta$  function expresses the dressed four-momenta conservation condition. For simplicity, we have also introduced the matrix element  $t_N$ , which is the sum over all possible realizations of the  $N$ th photon process,

$$\begin{aligned}
 t_N \equiv & t_N(p_{e^-} \lambda_{e^-}, p_{e^+} \lambda_{e^+}; q_f \lambda_f, q_i \lambda_i) \\
 = & \sum_L C_{N-L}^\mu(p_{e^-} \lambda_{e^-}, p_{e^+} \lambda_{e^+}) \tilde{D}_{\mu\nu}(\bar{q}_i - \bar{q}_f + Lk) \\
 & \times \mathcal{F}_L^v(q_f \lambda_f, q_i \lambda_i). \quad (28)
 \end{aligned}$$

This is represented schematically in Fig. 2. Introducing  $N_1, N_2, N_3$ , and  $N_4$  as numbers of photons that are absorbed from the laser field by the reaction particles and  $N'_1, N'_2, N'_3$ , and  $N'_4$  as numbers of photons that are emitted back to the laser field, we find out that the net number of photons that are exchanged with the field by the nucleus is  $L = N_1 + N_2 - N'_1 - N'_2$ , and similarly for the pair,  $M = N_3 + N_4 - N'_3 - N'_4$ . Hence,

the net number of photons that are exchanged with the laser field by all particles, which specifies the  $N$ -photon channel for pair creation, equals  $N = N_1 + N_2 + N_3 + N_4 - N'_1 - N'_2 - N'_3 - N'_4$ , and, moreover, it must be positive in order for pair creation to take place. It is clear from this picture that for very large  $N$ , the matrix element  $t_N$  is the sum of a huge number of amplitudes corresponding to elementary diagrams that have a specific sequence of absorbed or emitted by the charged particles laser photons. This will lead later on to very rapid oscillations of probability rates. Hence, these oscillations can be interpreted as the interference between probability amplitudes corresponding to different paths which lead, however, to the same final state.

### C. Probability rates

The probability rate of pair production due to the absorption of  $N$ -laser photons is defined as

$$W_N = \sum_{\{\lambda\}} \int \frac{V d^3 q_f}{(2\pi)^3} \frac{V d^3 p_{e^-}}{(2\pi)^3} \frac{V d^3 p_{e^+}}{(2\pi)^3} \frac{|S_{\text{fi}}^{(N)}|^2}{T}, \quad (29)$$

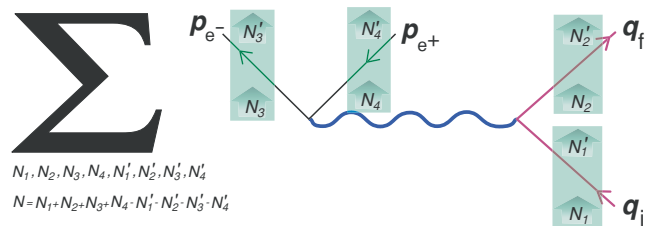


FIG. 2. (Color online) Schematic representation of the matrix element  $t_N$  [Eq. (28)], where  $N$  is the net number of photons being exchanged with the laser field by the reaction particles. While  $N_1, N_2, N_3$ , and  $N_4$  denote numbers of photons that are absorbed from the laser field,  $N'_1, N'_2, N'_3$ , and  $N'_4$  stand for photons that are emitted by the particles into the field. Thus,  $N = N_1 + N_2 + N_3 + N_4 - N'_1 - N'_2 - N'_3 - N'_4$ . Let us emphasize that the thick lines describing the nuclear and electron-positron currents in Fig. 1 are represented here as thin lines dressed by the laser field.

where the quantity  $|S_{\bar{n}}^{(N)}|^2/T$  describes the corresponding transition rate between well-defined momentum and spin states of particles and where integration over the density of final momentum states for nuclei  $Vd^3q_f/(2\pi)^3$ , electrons  $Vd^3p_{e^-}/(2\pi)^3$ , and positrons  $Vd^3p_{e^+}/(2\pi)^3$  is carried out. To simplify the notation, we have introduced the symbol

$$\sum_{\{\lambda\}} = \frac{1}{2} \sum_{\lambda_i=\pm} \sum_{\lambda_f=\pm} \sum_{\lambda_{e^-}=\pm} \sum_{\lambda_{e^+}=\pm}, \quad (30)$$

where  $\frac{1}{2} \sum_{\lambda_i=\pm}$  arises from the averaging of  $|S_{\bar{n}}^{(N)}|^2/T$  with respect to the initial spin degrees of freedom while the rest corresponds to the summation over the final spin degrees of freedom. Then, from the matrix element  $S_{\bar{n}}^{(N)}$  [Eq. (27)], we obtain by the usual methods (see, for instance, Ref. [56]) that

$$\frac{|S_{\bar{n}}^{(N)}|^2}{T} = \frac{\mathcal{Z}^2 \alpha^2 m_e^2 M_N^2 c^9}{2\pi^3 V^3} \frac{|t_N|^2}{E_{q_i} E_{q_f} E_{p_{e^-}} E_{p_{e^+}}} \times \delta(\bar{q}_i - \bar{q}_f - \bar{p}_{e^-} - \bar{p}_{e^+} + Nk). \quad (31)$$

As one can conclude from Eqs. (29) and (31), to perform the corresponding integrations by means of the  $\delta$  function is not straightforward. With the reference to our definition of the laser-dressed momenta (7), let us find first the Jacobian  $|\partial \bar{p}_{e^+}/\partial \bar{p}_{e^+}|$ ,

$$J(\bar{p}_{e^+}) \equiv \left| \frac{\partial \bar{p}_{e^+}}{\partial \bar{p}_{e^+}} \right| = \left| 1 - \frac{(m_e c)^2 \mu^2}{4k \cdot \bar{p}_{e^+}} \frac{k^0}{\bar{p}_{e^+}^0} \right|, \quad (32)$$

that enables us to perform the integral over  $d^3p_{e^+}$  exactly. This leads to

$$W_N = \frac{\mathcal{Z}^2 \alpha^2 m_e^2 M_N^2 c^9}{2\pi^3} \sum_{\{\lambda\}} \int \frac{d^3q_f}{E_{q_f} E_{q_i}} \frac{d^3p_{e^-}}{E_{p_{e^-}} E_{p_{e^+}}} J(\bar{p}_{e^+}) \times |t_N|^2 \delta(\bar{q}_i^0 - \bar{q}_f^0 - \bar{p}_{e^-}^0 - \bar{p}_{e^+}^0 + Nk^0), \quad (33)$$

where one has to remember that  $\bar{p}_{e^+} = \bar{q}_f - \bar{q}_i - \bar{p}_{e^-} + Nk$  must obey the related on-mass-shell condition,  $\bar{p}_{e^+}^2 = (\bar{m}_e c)^2$  and also that any quantity which encounters the dependence on  $\bar{p}_{e^+}$  or  $p_{e^+}$  in Eq. (33) is in fact the function of the other momenta. In particular, it also relates to the argument of the remaining one-dimensional  $\delta$  function, and so we rewrite it using the well-known property

$$\delta[f(x)] = \sum_{\ell} \frac{1}{|f'(x^{(\ell)})|} \delta[x - x^{(\ell)}], \quad (34)$$

where  $x^{(\ell)}$  is the  $\ell$ th solution to the equation  $f(x) = 0$ ; with this substitution, one of the remaining integrals in Eq. (33) becomes trivial. To see this better, we write that  $d^3p_{e^-} = d\Omega_{p_{e^-}} |p_{e^-}| p_{e^-}^0 dp_{e^-}^0$  (and similarly for  $d^3q_f$ ), and then, in Eq. (33), we perform the related one-dimensional integral with respect to  $dp_{e^-}^0$ , making use of the aforementioned property. This yields

$$W_N = \frac{\mathcal{Z}^2 \alpha^2 m_e^2 M_N^2 c^6}{2\pi^3} \sum_{\ell} \sum_{\{\lambda\}} \int dE_{q_f} d\Omega_{q_f} d\Omega_{p_{e^-}} \times |t_N|^2 \left. \frac{|q_f| |p_{e^-}| J(\bar{p}_{e^+})}{E_{q_i} E_{p_{e^+}} D(p_{e^-})} \right|_{E_{p_{e^-}} = E_{p_{e^-}}^{(\ell)}}, \quad (35)$$

where  $E_{p_{e^-}}^{(\ell)}$  is the  $\ell$ th solution of the energy conservation relation that follows from Eq. (33) (Appendix), whereas the denominator  $D(p_{e^-})$  is found to be

$$D(p_{e^-}) = \left| -1 + \frac{p_{e^-}^0}{\bar{p}_{e^+}^0} \frac{p_{e^-} \cdot \bar{p}_{e^+}}{p_{e^-}^2} + \frac{(m_e c)^2 \mu^2}{4(k \cdot p_{e^-})} \times \left( k^0 - p_{e^-}^0 \frac{k \cdot p_{e^-}}{p_{e^-}^2} \right) \left( k^0 - \frac{k \cdot \bar{p}_{e^+}}{\bar{p}_{e^+}^0} \right) \right|. \quad (36)$$

As anticipated previously, the function that must be integrated in (35) encounters huge oscillations. This makes the numerical evaluation of the probability rate  $W_N$  rather demanding. Let us note that the preceding oscillating function has essentially the meaning of the triply differential probability rate of  $N$ -photon pair production for the case when the value of energy transfer from the nucleus and orientations of the nucleus and the electron are known,  $R_N^{(\ell)}(q_f, \hat{p}_{e^-})$ . The definition

$$W_N = \sum_{\ell} \int dE_{q_f} d\Omega_{q_f} d\Omega_{p_{e^-}} R_N^{(\ell)}(q_f, \hat{p}_{e^-}), \quad (37)$$

as compared to Eq. (35), enables us to explicitly write the formula

$$R_N^{(\ell)}(q_f, \hat{p}_{e^-}) \equiv \frac{d^3 W_N^{(\ell)}}{dE_{q_f} d\Omega_{q_f} d\Omega_{p_{e^-}}} = \frac{\mathcal{Z}^2 \alpha^2 m_e^2 M_N^2 c^6}{2\pi^3} \times \sum_{\{\lambda\}} |t_N|^2 \left. \frac{|q_f| |p_{e^-}| J(\bar{p}_{e^+})}{E_{q_i} E_{p_{e^+}} D(p_{e^-})} \right|_{E_{p_{e^-}} = E_{p_{e^-}}^{(\ell)}}. \quad (38)$$

Let us note that the second line in this equation, if one neglects  $\sum |t_N|^2$ , is proportional to the nonrelativistic density of final states. For this reason, we refer to it as the laser-modified density of final states  $\mathcal{G}^{(\ell)}(q_f, \hat{p}_{e^-})$ ,

$$\mathcal{G}^{(\ell)}(q_f, \hat{p}_{e^-}) = \left. \frac{|q_f| |p_{e^-}| J(\bar{p}_{e^+})}{E_{q_i} E_{p_{e^+}} D(p_{e^-})} \right|_{E_{p_{e^-}} = E_{p_{e^-}}^{(\ell)}}. \quad (39)$$

We further remark that the same differential rate would be obtained if, instead of the electron orientation, the positron orientation was known. In both instances, we can explicitly study the effect of energy (or momentum) transfer from a nucleus which is the main subject of this article.

#### D. Massive nucleus approximation

In most theoretical works so far on the electron-positron pair production in laser-nucleus collisions, one of the key assumptions was to treat a nucleus as an infinitely heavy particle. Such a situation is not met, however, in real life. The question to be asked is: How do we approximately account for the finite mass of the recoil nucleus, which is indeed heavy?

Intuitively, one can expect that the motion of such a nucleus would not be affected by the laser field rather than at the instant of a collision, when the pair is produced; in other words, the effect of the electromagnetic field on the nucleus wave function would be neglected. In this case, the nucleus is described by a field-free plane wave, which corresponds to Eq. (2), if  $A_0 = 0$ . Such a heavy nucleus is not dressed by the field, so it carries the

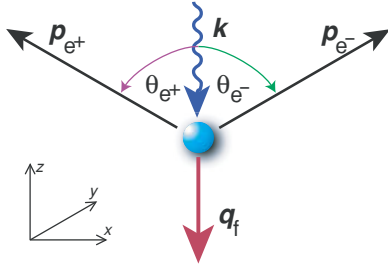


FIG. 3. (Color online) Geometry of the symmetric equal energy sharing between an electron and a positron that are created in a nucleus–laser-field collision, in a reference frame where a nucleus is at rest long before the collision takes place. Only asymptotic momenta, which would be measured outside the laser focus in the chosen frame of reference, are depicted. For this geometry,  $|\mathbf{p}_{e^-}| = |\mathbf{p}_{e^+}|$  and  $\theta_{e^-} = \theta_{e^+}$ .

momenta  $q_i$  and  $q_f$  before and after collision, respectively. In the following, we discuss briefly how good this approximation is in comparison with the exact results based on the formulas derived in the previous section. In the case of a massive recoil nucleus, all the formulas derived previously stay the same but one has to put  $A_0 = 0$  correspondingly.

### III. SYMMETRIC GEOMETRY

We start our investigations on triply differential probability rates in the process of electron-positron pair production [Eq. (38)], considering the head-on nucleus-laser collision such that it leads to equal energy sharing between the created particles. The corresponding coplanar kinematics in the reference frame related to a nucleus initially at rest is depicted in Fig. 3; in other words, it is understood that  $\mathbf{q}_i = \mathbf{0}$ . As one can see from Fig. 3, we assume that the plane-wave laser field propagates along the  $z$  axis, with the wave vector  $\mathbf{k} = -(\omega/c)\mathbf{e}_z$ . For coplanar symmetric kinematics, the created electron and positron are detected with equal energies symmetrically with respect to the field direction (if  $\theta$  measures the polar angle, then  $\theta_{e^+} = \theta_{e^-}$ ), and therefore the nucleus is accelerated along the  $z$  axis. As is anticipated in Fig. 3, we consider the case when the recoiling nucleus is detected with momentum  $q_{f,z} < 0$ . In this case, the minimal number of photons that are absorbed from the laser field in order to create pairs is

$$N_{\text{th}} = \frac{4(\bar{m}_e c)^2 - (\bar{q}_i - \bar{q}_f)^2}{2k \cdot (\bar{q}_i - \bar{q}_f)}, \quad (40)$$

which has been derived using the conservation relation of four-momenta. This equation holds also for a very massive nucleus if the dressed momenta  $(\bar{q}_i, \bar{q}_f)$  are replaced by  $(q_i, q_f)$ . Let us emphasize that  $N_{\text{th}}$  corresponds to the smallest possible energy of created particles in the laser focus. Thus, the energy threshold for pair production is much higher than the field-free energy threshold,  $2m_e c^2$ , as we illustrate in Sec. III A.

A number of theoretical studies have been performed to investigate the electron-positron pair creation in the process of laser-nucleus collisions assuming that the colliding nucleus is infinitely massive (i.e., neglecting the nuclear recoil). In the present article, we employ a more accurate approach

by taking into account the finite mass of the nucleus. In this context, it is important to realize that in this more realistic situation the pair creation cannot occur without the nuclear recoil (see the Appendix). At the same time, based on our earlier results for a linearly polarized laser field assuming the infinite mass of a nucleus [3,42], one can expect that the pairs would be preferably created in the coplanar symmetric configuration. Thus, we analyze this case more closely using our exact treatment of a nucleus in the laser field.

#### A. Parallel case

With reference to our earlier works [3,42], we investigate in the following a linearly polarized laser field, with the polarization vector in the  $xz$  plane, in which the ellipticity parameter is zero,  $\delta = 0$ . For a relativistic nucleus counterpropagating toward a laser pulse of linear polarization, it holds that the laser field remains linearly polarized but its frequency becomes Doppler upshifted by a factor of  $\gamma_D = 2\gamma$  for sufficiently large  $\gamma$ , where  $\gamma$  is the relativistic Lorentz factor. For the figures discussed in the following, we take  $\omega = 0.01m_e c^2$  (in the chosen frame of reference) and the parameter  $\mu$  describing the laser-field strength,  $\mu = 100$ . As a colliding nucleus we choose isotope of Ne ( $Z = 10$ ), with ten protons and nine neutrons and with a total spin of  $1/2$ . Moreover, the results presented here are obtained taking into account at most five-laser-photon exchange between a nucleus and a pair,  $-5 \leq L \leq 5$  [for the definition of the respective photon exchange, see Eq. (28)].

In Fig. 4, we show kinematical parameters for the process being considered as functions of nucleus momentum transfer

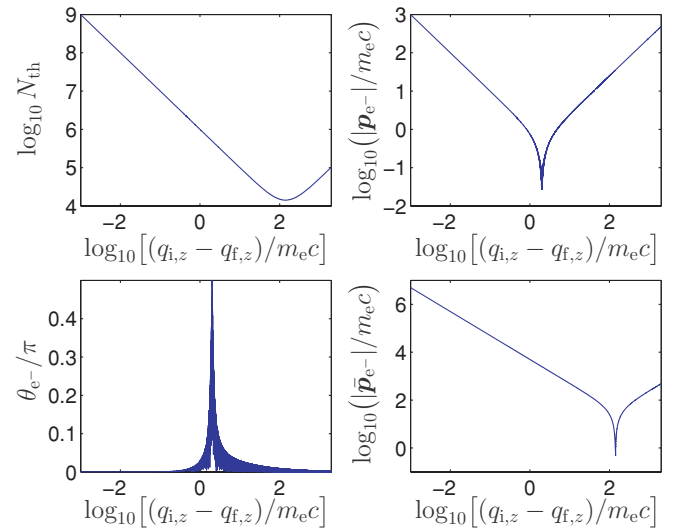


FIG. 4. (Color online) For a laser source such that  $\omega = 0.01m_e c^2$  and  $\mu = 100$  colliding with a beam of Ne nuclei ( $Z = 10$ ), kinematical parameters for the process of pair creation in the configuration depicted in Fig. 3 as functions of the momentum transfer from the nucleus  $(q_{i,z} - q_{f,z})$  are presented. The top left panel shows the corresponding dependence of the minimum number of absorbed laser photons necessary for the pair creation to take place,  $N_{\text{th}}$ ; the bottom left panel shows the dependence of the polar angle of a detected electron  $\theta_{e^-}$  (or positron); the right panels present the respective dependence of electron (positron) asymptotic and dressed momenta (top and bottom panels, respectively).

in the counterpropagating setup (Fig. 3). At this point, let us only mention that for the present geometry there is only one solution to the four-momenta conservation condition, and so in Eq. (34) there is only one term. For this reason, we keep in the following the notation  $R_N(\mathbf{q}_f, \hat{\mathbf{p}}_{e^-})$  for the corresponding triply differential probability rate and  $\mathcal{G}(\mathbf{q}_f, \hat{\mathbf{p}}_{e^-})$  for the density of final states. The top left panel displays the dependence of threshold number of photons that is necessary for the  $e^-e^+$  pair creation,  $N_{\text{th}}$ , on the momentum transfer from the nucleus ( $q_{i,z} - q_{f,z}$ ) in units of  $m_e c$ . Further, the bottom left panel presents the similar dependence of the polar detection angle of an electron (positron)  $\theta_{e^-}$ , while the right panels refer to the electron (positron) momentum measured either outside of (top panel) or in (bottom panel) the laser focus. One can see from the top left panel that in the limiting case of zero-momentum transfer from the nucleus, the number of absorbed laser photons becomes infinite, which reflects the fact that such a transition is energetically forbidden. Then, with growing ( $q_{i,z} - q_{f,z}$ ) up to around  $100m_e c$ , the minimum number of laser photons that must be absorbed in order to create pairs drops significantly (however, it is still larger than the field-free energy threshold for pair production, as explained previously). As one can expect, an additional momentum kick from the nucleus does result in an increasing probability rate of pair creation, which we illustrate in the next figure (cf. Fig. 5). At this point, let us only mention that the smallest value of  $N_{\text{th}}$  does not necessarily correspond to the maximum of the triple probability rate of pair production; we rather observe (comparing Figs. 4 and 5) that the rate is maximum for such momentum transfer from the nucleus that the electron (positron) asymptotic momentum  $|\mathbf{p}_{e^-}|$  is minimum. One can see from Fig. 4 that this takes place when electrons and positrons are detected perpendicularly to the

laser-field propagation direction. This indicates that the most favorable process in this configuration is such that the total momentum of absorbed photons is preferably transferred to the nucleus.

Next, we examine the dependence of triply differential probability rates for electron-positron pair creation on the momentum transfer from the Ne nucleus in the configuration presented in Fig. 3. In Fig. 5, we show the corresponding results for the case when 10- [panels (a) and (c)] and 1000-above-threshold laser photons [panels (b) and (d)] are absorbed. For our purpose let us denote the number of laser photons absorbed above the electron-positron pair-creation threshold as  $S = N - N_{\text{th}}$ , meaning that in the present case we consider the situation when  $S$  is either 10 or 1000. Here,  $N_{\text{th}}$  depends on the momentum transfer ( $q_{i,z} - q_{f,z}$ ) the way displayed in Fig. 4. Looking at panels (a) and (b) of Fig. 5, one can see very rapid and dense oscillations of the corresponding rates, discussed already in Sec. II B. Rather than that, we observe a clear qualitative difference between both panels. For  $S = 10$  [panel (a)], the triply differential probability rates exhibit the so-called plateau structure, which means the flat dependence of the probability rates over the finite range of momentum transfer from the nucleus ( $q_{i,z} - q_{f,z}$ ), which is not observed in the case when  $S = 1000$  [panel (b)]. It is a well-known fact that similar plateaus are observed in multiphoton ionization spectra of photoelectrons [57]. While in multiphoton ionization such structures are believed to originate from the rescattering of ionized electrons by an ionic core under the influence of the laser field [57,58], the similar explanation does not apply here; this is due to the fact that our theoretical approach is based on the first-order Born approximation. The appearance of the plateau in the probability rates of pair creation by 10-above-threshold-photon absorption, shown in Fig. 5(a), is related to a very strong modification of the density of final states  $\mathcal{G}(\mathbf{q}_f, \hat{\mathbf{p}}_{e^-})$  by the presence of the laser field. The density of final states as a function of the momentum transfer from the nucleus in the case when  $S = 10$  is presented in Fig. 5(c). We see in this panel that  $\mathcal{G}(\mathbf{q}_f, \hat{\mathbf{p}}_{e^-})$  exhibits a very deep minimum for momentum transfer around  $2m_e c$ , which exactly corresponds to the region where the respective plateau in panel (a) is observed. While in the case of 10-above-threshold-photon absorption, the density of final states changes by two orders of magnitude on the scale where ( $q_{i,z} - q_{f,z}$ ) changes from  $2m_e c$  to  $10m_e c$ . In the case of 1000-above-threshold photon absorption [panel (d)],  $\mathcal{G}(\mathbf{q}_f, \hat{\mathbf{p}}_{e^-})$  changes by much less than one order of magnitude. Such a rapid [panel (c)] versus slow [panel (d)] dependence of  $\mathcal{G}(\mathbf{q}_f, \hat{\mathbf{p}}_{e^-})$  on the nucleus momentum transfer ( $q_{i,z} - q_{f,z}$ ) results in the inflection [panel (a)] or in an abrupt decrease [panel (b)] of the envelope of triply differential probability rates with changing ( $q_{i,z} - q_{f,z}$ ) from  $2m_e c$  to  $10m_e c$ . Here, we should also mention that in the first case the density of final states oscillates with a small amplitude as a function of ( $q_{i,z} - q_{f,z}$ ), which manifests itself in Fig. 5(c) as a bold line, but in the second case, Fig. 5(d), the amplitude of such oscillations is even smaller.

At this point let us comment on the validity of the heavy nucleus approximation. We have compared the results for the triply differential probability rates assuming that the Ne nucleus is massive enough, so one can disregard dressing it by the laser field as discussed already in Sec. II D, with

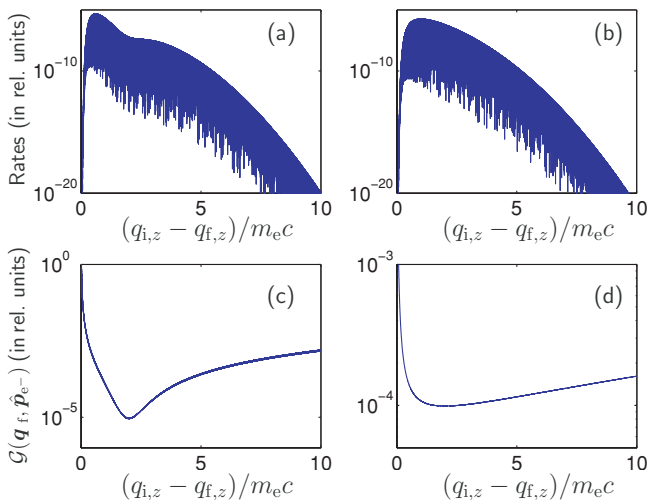


FIG. 5. (Color online) Dependence of triply differential probability rates (a), (b) and of the density of final states  $\mathcal{G}(\mathbf{q}_f, \hat{\mathbf{p}}_{e^-})$  (c), (d) on momentum transfer from the recoil nucleus ( $q_{i,z} - q_{f,z}$ ) (in units of  $m_e c$ ) in the case when 10- and 1000-above-threshold laser photons are absorbed in order to produce pairs [panels (a, c) and (b, d), respectively; the head-on configuration presented in Fig. 3 is considered].

the results of our exact treatment of the Ne nucleus in the laser field (for the cases when we have at most five- and at most ten-photon exchange between the nucleus and the laser field,  $-5 \leq L \leq 5$  and  $-10 \leq L \leq 10$ , respectively) that is along the lines presented in Secs. II B and II C. In each case, we observe very dense and rapid oscillations of the differential probability rates with the nucleus momentum kick ( $q_{i,z} - q_{f,z}$ ), as seen in Fig. 5. At this point, let us note that such dense oscillations are typical for a multiphoton pair creation characterized by a small frequency of the laser field  $\omega$ ; however, they smooth out with increasing  $\omega$ . Despite these oscillations, which are uncorrelated for different  $L$ 's, the respective envelopes turned out to be almost identical. This follows from the fact that the correction to the rest-mass energy squared of the nucleus, due to its dressing by the laser field, equals  $(Z\mu m_e c^2)^2/2$ , which is much smaller than the rest-mass energy squared of the nucleus itself. Therefore, we conclude that one can neglect the influence of the laser field on the nucleus, unless one considers pair creation by the impact of very light particles on the laser beam. At the same time, it should be emphasized that the calculations are performed under certain general approximations (such as, for instance, a plane-wave laser-field approximation) which prevent the theory employed to be quantitatively predictive on such small details like dense oscillations observed, for instance, in Fig. 5.

In Fig. 6, we show the above-threshold triply differential probability rates (in the  $\log_{10}$  scale) as functions of the number of laser photons above the electron-positron pair-creation threshold,  $S$ , for three different values of momentum transfer from the colliding nucleus:  $1.89m_e c$  [blue (upper) curve],

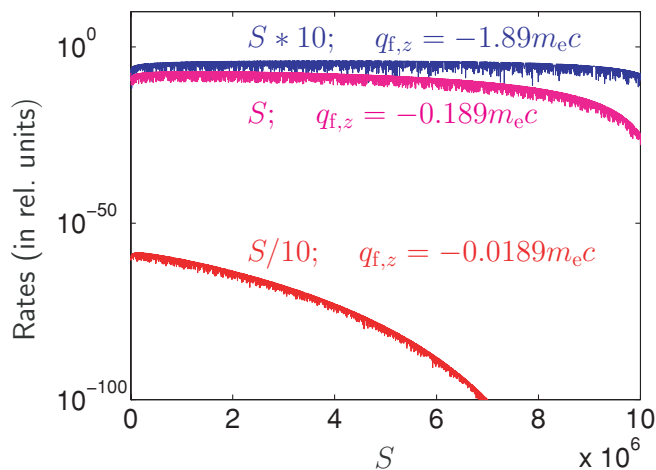


FIG. 6. (Color online) Triply differential probability rates vs the number of above-threshold-laser-photons  $S$  that are absorbed in order to produce electron-positron pairs [in the head-on collision setup (Fig. 3)] for the fixed momentum transfer from the recoil nucleus:  $1.89m_e c$  [blue (upper) curve],  $0.189m_e c$  [pink (middle) curve], and  $0.0189m_e c$  [red (lower) curve]. The triply differential probability rates are presented on the  $\log_{10}$  scale. For the largest momentum transfer (upper curve), the horizontal axis should be scaled by a factor of 10, while for the smallest transfer (lower curve), the same axis must be scaled by 1/10.

$0.189m_e c$  [pink (middle) curve], and  $0.0189m_e c$  [red (lower) curve]. One should be aware that the horizontal scale should be multiplied by ten in the case of the biggest momentum transfer from the nucleus [blue (upper) curve] and divided by ten in the case of the smallest momentum transfer [red (lower) curve] that are presented in this figure. As one can see here, the probability rates of pair creation show a dramatic increase with increasing momentum transfer from the nucleus ( $q_{i,z} - q_{f,z}$ ); that is, a change in ( $q_{i,z} - q_{f,z}$ ) of only one order of magnitude induces an increase in the rate of several orders of magnitude (see lower vs middle and upper curves). However, what is not shown here is that for larger ( $q_{i,z} - q_{f,z}$ ) the probability rates start rapidly decreasing. To understand this better, let us note that in the case plotted as the red (lower) curve here there is approximately  $10^8$  laser photons necessary for the pair creation to take place (see Fig. 4, panel specifying  $N_{th}$ ), while the number of the above-threshold photons  $S$  that are absorbed from the laser field is of the order of  $10^5$ . It means that we deal here with the case nearly above the reaction threshold ( $S \ll N_{th}$ ). Most importantly, in this case the number of absorbed laser photons  $N$  ( $N = N_{th} + S$ ) is very large, which results in a small probability of pair creation. The pink (middle) curve, on the other hand, corresponds to  $N_{th}$  and  $S$  of the order of  $10^7$  and  $10^6$  photons, while for the blue (upper) curve we have  $10^6$  and  $10^7$  photons, respectively. In both of these cases, we can talk about the pair creation that is relatively far beyond the threshold and with substantially smaller  $N$  than in the previous case. Thus, the respective rates are much bigger than the one plotted in red (lower curve). Increasing ( $q_{i,z} - q_{f,z}$ ) even more, we observe in Fig. 4 that  $N_{th}$  does not change rapidly any longer (and hence also  $N$ ), which explains the saturation of the probability rates with growing ( $q_{i,z} - q_{f,z}$ ). As one can see in Fig. 4, at some point  $N_{th}$  even starts to increase (and so  $N$  does), which results in decreasing the probability rates of pair production. Let us emphasize that such a dependence of the probability rates on the momentum transfer from the nucleus is typical also for other geometries of the reaction particles. It also confirms that, taking into account the recoil imparted on the colliding nucleus, one can significantly enhance the probability rates of the electron-positron pair creation. The point being that the  $e^-e^+$  pairs can be created if there is enough energy supplied by both the laser field and by the colliding nucleus. The more energy is transferred from the nucleus, the fewer laser photons  $N$  have to be absorbed from the laser field (for momentum transfer less than  $100m_e c$ ) in order to produce pairs. This results in a tremendous increase in the probability rates of the process of pair creation, however, with a tendency to become saturated, as discussed previously.

In closing our considerations on pair creation via head-on laser-nucleus collisions in this configuration let us mention that similar results have been obtained for even heavier nuclei, like  $Pb^{82+}$  having 82 protons and 125 neutrons ( $Z = 82$ ). The fact that the results for  $Ne^{10+}$  and  $Pb^{82+}$  are indeed very similar can be expected since for both nuclei the energy correction that originates from the dressing by the laser field,  $(Z\mu m_e c^2)^2/2$ , is still small in comparison with the nucleus rest-mass energy squared. For this reason, we do not present here the corresponding results for  $Pb^{82+}$ .

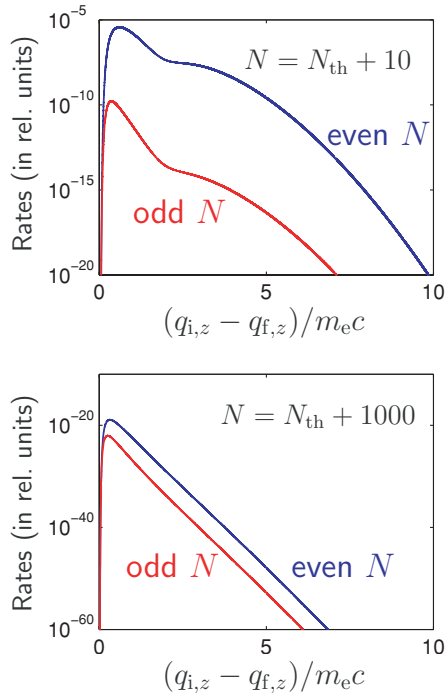


FIG. 7. (Color online) The same as in panels (a) and (b) of Fig. 5 (here, top and bottom panels, respectively) for the case when the laser-field polarization vector is along the  $y$  axis (see Fig. 3).

### B. Perpendicular case

In this section, we consider the case of equal energy sharing between an electron and a positron that are created in the head-on laser-nucleus collisions, as presented in Fig. 3, for the case when the ellipticity parameter of the laser field [see Eq. (4)] is  $\delta = \pi/2$ ; in other words, the only difference in comparison with the situation considered in the previous section is that the polarization of the laser field is along the  $y$  axis. Figure 7 shows the dependence of triply differential probability rates for pair creation on momentum transfer from the colliding nucleus for the case of 10- and 1000-above-threshold-photon pair production (top and bottom panels, respectively). This time, contrary to the previous case, we observe a very pronounced difference between the results for even- and odd-laser-photon pair production. This feature of probability rates can be understood based on formulas describing the electron-positron and nuclear currents [see Eqs. (17)–(19), (21), (23)–(25)]. For  $\delta = \pi/2$ , the first argument of the generalized Bessel functions is in each case equal to zero [see Eqs. (21) and (23)], meaning that only the even-photon-number Bessel functions ( $B_N$ , with  $N$  being an even number) enter into the coefficients  $C_N^\mu$  and  $\mathcal{F}_N^\nu$  [see Eqs. (24) and (25)]. This, however, does not mean that only an even number of photons can be exchanged between particles and the laser field. Let us note that in the formulas defining the Fourier coefficients  $C_N^\mu$  and  $\mathcal{F}_N^\nu$  there are terms with  $N, N \pm 1$  and  $N \pm 2$  photon numbers, while the even- $N$  terms are multiplied by  $\mu^2$  the odd- $N$  terms are only multiplied by  $\mu$ ; hence, the rates of pair production with absorption of an even number of photons should be approximately  $\mu^2$  times larger than the rates of pair production with absorption of an

odd-photon number. In the case illustrated in Fig. 7, that is for  $\mu = 100$ , one should observe therefore a four-order-of-magnitude difference between these two cases. This agrees quite well with the results presented in Fig. 7.

Let us note that in the present geometry, the rates of near-threshold pair production (top panel) are of comparable magnitude as those for the geometry considered in the preceding section. However, by comparing both panels in Fig. 7, one can conclude that with increasing the number of above-threshold photons (bottom panel) the rates decrease in magnitude dramatically, which has not been observed for the previous geometry. Moreover, by looking at Fig. 7, one could get an impression that this time the differential rates depend smoothly on the momentum transfer from the nucleus; that is, they do not exhibit similar interference oscillations as functions of  $(q_{i,z} - q_{f,z})$ . In fact, just like for the previous geometry, each curve in Fig. 7 is an oscillating function of the momentum transfer  $(q_{i,z} - q_{f,z})$  but with a very small amplitude.

### C. Elliptic polarization

For the configuration setup analyzed in Sec. III A, we concentrate now on the dependence of triply differential probability rates of pair creation  $R_N(\mathbf{q}_f, \hat{\mathbf{p}}_{e^-})$  on the polarization of the laser field; in other words, we take this time the ellipticity parameter such that  $\delta \neq 0$  and  $\delta \neq \pi/2$ . Figures 8 and 9 show the dependence of the respective probability rates on momentum transfer from the nucleus  $(q_{i,z} - q_{f,z})$  for 10- and 1000-above-threshold-photon pair production (top and

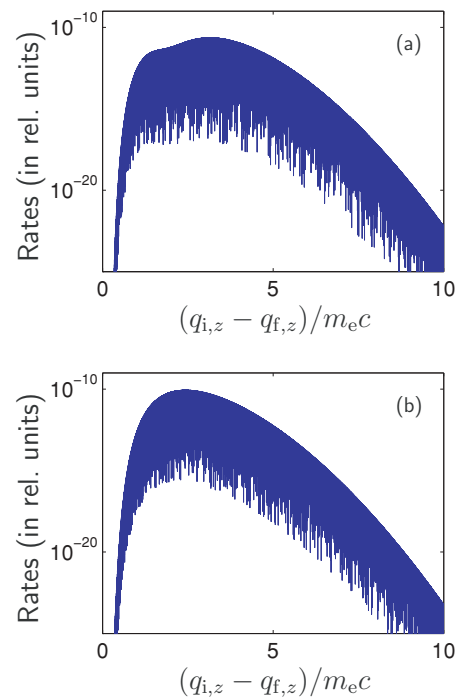


FIG. 8. (Color online) For the same parameters as in Sec. III A and for the ellipticity parameter  $\delta = 0.005\pi$ , the triply differential probability rates  $R_N(\mathbf{q}_f, \hat{\mathbf{p}}_{e^-})$  as functions of momentum transfer from the nucleus. The top and bottom panels correspond to 10- and 1000-above-threshold-photon pair production.

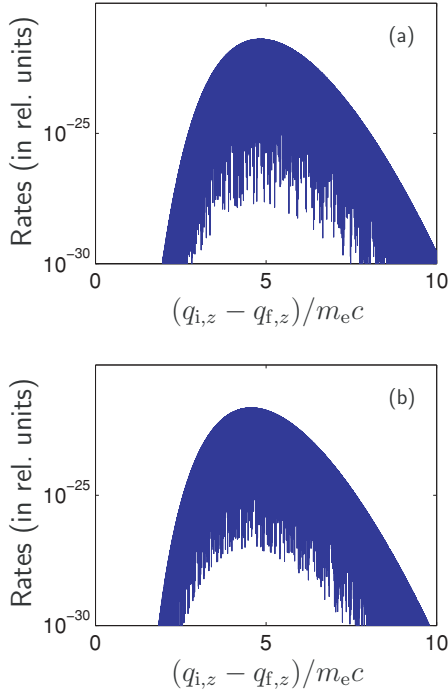


FIG. 9. (Color online) The same as in Fig. 8 but for the ellipticity parameter  $\delta = 0.01\pi$ .

bottom panels, respectively) for two cases, when  $\delta = 0.005\pi$  (Fig. 8) and  $\delta = 0.01\pi$  (Fig. 9). One can see from these figures that the probability rates depend strongly on the polarization of the colliding laser beam. If one compares these figures with similar results presented in Fig. 5, panels (a) and (b) appropriately, for the case of the linear polarization when  $\delta = 0$ , one can see a very dramatic decrease of the differential probability rates when  $\delta$  increases. For even higher  $\delta$ , for which however we do not present the respective results here, the differential probability rates become negligibly small (already for  $\delta = 0.1\pi$ , they become smaller than  $10^{-300}$  in relativistic units, and even less for  $\delta = 0.25\pi$ , which corresponds to a circular polarization of the laser field). Such a dramatic dependence of the probability rates on the polarization of the laser field is not usually observed in other multiphoton processes. One should remember, however, that we deal here with a multiphoton process, in which millions of photons are absorbed; this explains such a dramatic dependence of the probability rates on the ellipticity of the laser field. At the same time, one can observe that the maximum of probability rates shifts toward higher momentum transfer from the nucleus with increasing  $\delta$ .

#### IV. ANGULAR DISTRIBUTIONS

Our foregoing investigations of pair production in the case of symmetric equal energy sharing between the created particles show the importance of nuclear recoil, which is imparted during the process, as was already suggested in our previous work [38]. Since the differential probability rates  $R_N^{(\ell)}(\mathbf{q}_f, \hat{\mathbf{p}}_{e^-})$  are maximal for nonzero momentum transfer from the nucleus, in the following we consider the situation when

the Ne nucleus is reflected in the direction of the laser-field propagation such that, in the reference frame where the nucleus is at rest before the collision takes place (meaning that  $\mathbf{q}_i = \mathbf{0}$ ), its momentum equals  $\mathbf{q}_f = -m_e c \mathbf{e}_z$ . This time, for the parameters analyzed in Sec. III A ( $\mu = 100, \omega = 0.01 m_e c^2, \delta = 0$ , and  $-5 \leq L \leq 5$ ), we fix the number of photons which are absorbed from the laser field,  $N = 1\,060\,000$ , to analyze the dependence of  $R_N^{(\ell)}(\mathbf{q}_f, \hat{\mathbf{p}}_{e^-})$  on the electron detection angles,  $\theta_{e^-}$  and  $\varphi_{e^-}$ .

In order to calculate the differential probability rates of pair production  $R_N^{(\ell)}(\mathbf{q}_f, \hat{\mathbf{p}}_{e^-})$  for a general configuration of the created particles, one has to start with solving the four-momentum conservation law given by the equation,

$$\bar{q}_i - \bar{q}_f - \bar{p}_{e^-} - \bar{p}_{e^+} + Nk = 0. \quad (41)$$

For the method of solving this equation, see the Appendix. Based on the preceding equation, one can check that the momenta of particles  $|\mathbf{p}_{e^-}|$  and  $|\mathbf{p}_{e^+}|$  do not depend on the electron azimuthal angle  $\varphi_{e^-}$ . Therefore, in Fig. 10, we present the electron and positron momenta (in units of  $m_e c$ ) as functions of the electron polar angle  $\theta_{e^-}$  (top and bottom panels, respectively), which follows from solving Eq. (41).

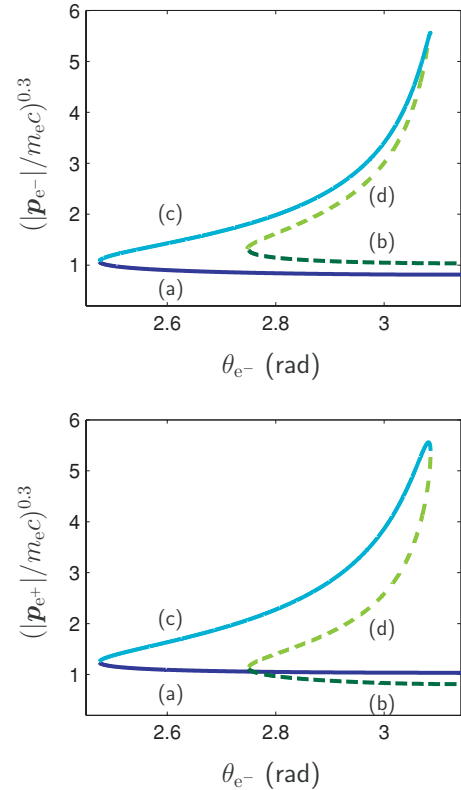


FIG. 10. (Color online) Dependence of the electron and positron momenta ( $|\mathbf{p}_{e^-}|$  and  $|\mathbf{p}_{e^+}|$ , respectively, in units of  $m_e c$ ) on the electron polar angle  $\theta_{e^-}$ , which follows from solving the four-momentum conservation equation, as shown in the Appendix. Low-energy particles are in sectors (a) and (b), marked as dark blue (solid dark gray) and dark green (dashed dark gray) curves respectively, while high-energy particles are in sectors (c) and (d) that are marked by light blue (solid light gray) and light green (dashed light gray) curves. Note that values of scaled momenta are raised to the power 0.3, which lowers them substantially.

One can see that for the chosen momentum transfer of the Ne nucleus and for the chosen number of absorbed laser photons, the particles are created predominantly in a window of  $\theta_{e^-}$  close to  $\pi$  or, in other words, they are mostly created in the direction of laser-field propagation. Besides, one can distinguish naturally different sectors in both panels in Fig. 10. While sectors (a) and (b) for  $\theta_{e^-} \in [2.5, \pi]$  and  $\theta_{e^-} \in [2.8, \pi]$ , respectively, correspond to the low-energy pairs created during the collision, sectors (c) and (d), for  $\theta_{e^-} \in [2.5, 3.1]$  and  $\theta_{e^-} \in [2.8, 3.1]$ , are related to the high-energy pairs. Therefore, one can see that these three electron polar angles, namely,  $\theta_{e^-}^{(1)} = 2.5$ ,  $\theta_{e^-}^{(2)} = 2.8$ , and  $\theta_{e^-}^{(3)} = 3.1$  mark the thresholds between different sectors for pair production. From Fig. 10, one notes that, with increasing the momentum of created particles, for  $\theta_{e^-}^{(1)}$ , the sectors (a) and (c) become open; for  $\theta_{e^-}^{(2)}$ , the sectors (b) and (d) are open; whereas for  $\theta_{e^-}^{(3)}$ , the high-energy sectors (c) and (d) become closed. This resembles the concept of channel closings that has been adapted recently in the nonrelativistic theory of ionization to explain enhancements in the photoelectron energy spectrum from negative ions. As has been demonstrated in Refs. [59–63], a dramatic enhancement (up to an order of magnitude) in the energy spectrum of ionized electrons is observed at multiphoton thresholds. As we present this in Fig. 11 for the zero azimuthal angle  $\varphi_{e^-} = 0$ , a similar enhancement of differential probability rates for the multiphoton pair creation  $R_N^{(\ell)}(\mathbf{q}_f, \hat{\mathbf{p}}_{e^-})$  is observed at the threshold between different sectors of created particles, which have been specified in Fig. 10. Even though the presented data (Fig. 11) are for the zero azimuthal angle, the probability rates for pair production exhibit a similar behavior for other angles  $\varphi_{e^-}$  close to 0 and  $\pi$ . Such a behavior is due to a significant increase of the laser-modified density of final states  $\mathcal{G}^{(\ell)}(\mathbf{q}_f, \hat{\mathbf{p}}_{e^-})$  near the respective thresholds.

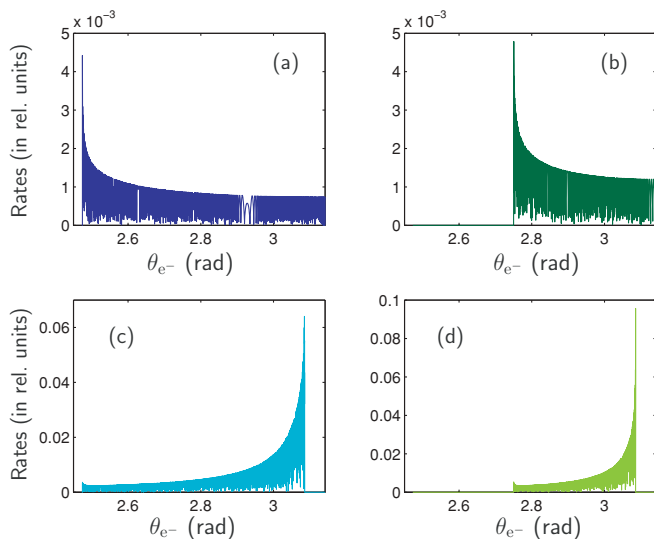


FIG. 11. (Color online) Triply differential probability rates of pair creation  $R_N^{(\ell)}(\mathbf{q}_f, \hat{\mathbf{p}}_{e^-})$  as functions of the electron polar angle  $\theta_{e^-}$ , measured with respect to the  $z$  axis. Each panel corresponds to the appropriate sector, labeled with the same letter in Fig. 10. The rates are raised to the power 0.3, which enhances the small values as compared with the large ones.

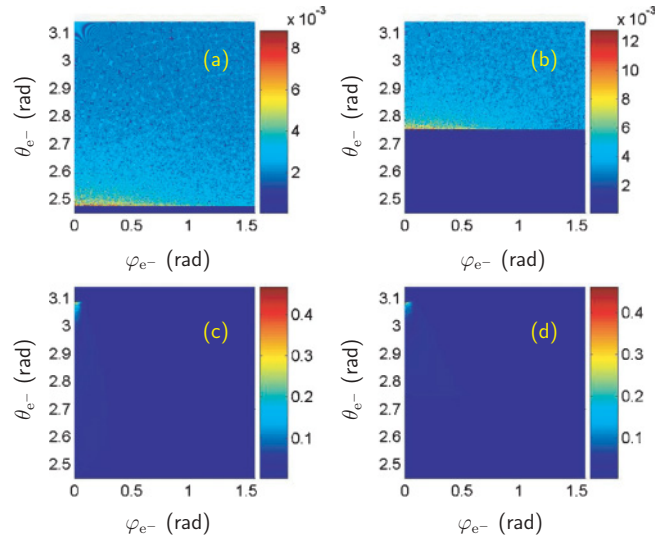


FIG. 12. (Color online) Angular maps of  $P_N^{(\ell)}(\mathbf{q}_f, \hat{\mathbf{p}}_{e^-})$ , as defined in Eq. (42), for different sectors specified in Fig. 10; each panel corresponds to the sector labeled in Fig. 10 with the same letter. Note that the values of  $P_N^{(\ell)}(\mathbf{q}_f, \hat{\mathbf{p}}_{e^-})$  in each panel have been raised to the power 0.25.

Let us now define a new quantity,

$$P_N^{(\ell)}(\mathbf{q}_f, \hat{\mathbf{p}}_{e^-}) = E_{p_{e^-}}^{(\ell)} R_N^{(\ell)}(\mathbf{q}_f, \hat{\mathbf{p}}_{e^-}), \quad (42)$$

that has the meaning of energy emitted per unit time in the form of electrons in the course of the laser-nucleus collision. For this reason, we call it in the following the electron energy transfer rate,  $P_N^{(\ell)}(\mathbf{q}_f, \hat{\mathbf{p}}_{e^-})$ . In Fig. 12, we show the respective color mappings of angular distributions of  $P_N^{(\ell)}(\mathbf{q}_f, \hat{\mathbf{p}}_{e^-})$ , where the values of  $P_N^{(\ell)}(\mathbf{q}_f, \hat{\mathbf{p}}_{e^-})$  have been raised to the power 0.25 for the visual effect. Each panel here corresponds to one sector (denoted by a letter), that has been specified when discussing Fig. 10. In particular, sectors (a) and (b) describe low-energy electrons, while sectors (c) and (d) are for high-energy electrons. One can see a qualitative difference between the production of low- and high-energy pairs. The high-energy electrons (and positrons) are created mainly in the plane spanned by the direction of the laser-field propagation (as follows already from Fig. 10) and by the polarization vector (in our configuration, in the  $xz$  plane). The low-energy electrons are emitted at slightly larger polar angles  $\theta_{e^-}$  but, most importantly, they are spread significantly with respect to the azimuthal angle  $\varphi_{e^-}$ . For low-energy pairs, which are better seen in panel (a), one can distinguish even a vortexlike structure, which we expect, however, not to be observed in an experiment.

For comparison, we present the results for an entirely asymmetric case, when the nucleus final momentum  $\mathbf{q}_f$  is such that  $|\mathbf{q}_f| = m_e c$ ,  $\theta_{q_f} = 0.9\pi$ , and  $\varphi_{q_f} = 0.4\pi$ . This time we draw the color mappings of  $P_N(\mathbf{q}_f, \hat{\mathbf{p}}_{e^-})$ , which is defined as

$$P_N(\mathbf{q}_f, \hat{\mathbf{p}}_{e^-}) = \sum_{\ell=1}^{\ell_{\max}} P_N^{(\ell)}(\mathbf{q}_f, \hat{\mathbf{p}}_{e^-}) \quad (43)$$

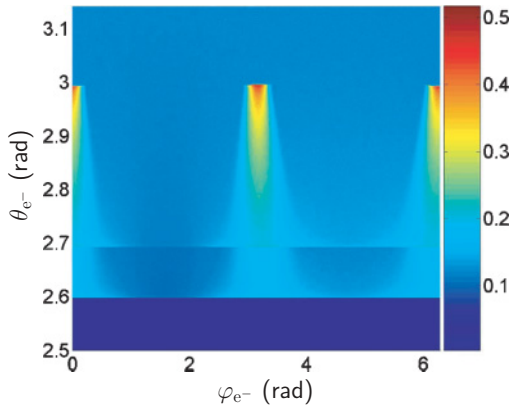


FIG. 13. (Color online) Angular maps of  $P_N(\mathbf{q}_f, \hat{\mathbf{p}}_{e^-})$ , defined by Eq. (43), for the case when the nucleus of final momentum  $|\mathbf{q}_f| = m_e c$  is measured at angles  $\theta_{q_f} = 0.9\pi$  and  $\varphi_{q_f} = 0.4\pi$ . For the visual effect, the values of  $P_N(\mathbf{q}_f, \hat{\mathbf{p}}_{e^-})$  have been raised to the power 0.1.

and is zero if  $\ell_{\max} = 0$ , meaning that there is no solution to the four-momentum conservation condition. The corresponding map of  $P_N(\mathbf{q}_f, \hat{\mathbf{p}}_{e^-})$  as a function of the electron polar and azimuthal angles,  $\theta_{e^-}$  and  $\varphi_{e^-}$ , is presented in Fig. 13. Let us note that for the visual purpose the values of  $P_N(\mathbf{q}_f, \hat{\mathbf{p}}_{e^-})$  have been raised to the power 0.1. From this figure one can distinguish different low-energy sectors with borders at approximately  $\theta_{e^-} = 2.6$  and  $2.7$ . These low-energy sectors, which are spread with respect to  $\varphi_{e^-}$ , constitute a background for the high-energy sectors being concentrated around the polarization vector of the laser field, that is, around  $\varphi_{e^-} = 0$  and  $\pi$ . This is analogous to the case discussed before, when the colliding nucleus (of the same energy) is detected in the propagation direction of the laser field. If one compares, however, the magnitudes of the rates presented in Figs. 12 and 13, one can see that in the previous case the values of  $P_N(\mathbf{q}_f, \hat{\mathbf{p}}_{e^-})$  are two or even three orders of magnitude bigger than in the present, nonsymmetric case. One can conclude, therefore, that the electron-positron pair production is more efficient in the configuration setup where the nucleus is reflected in the direction of the laser wave propagation, which is the case we have thoroughly analyzed in this article.

## V. TOTAL RATES

A desirable question to be asked is whether the nuclear recoil modifies the probability rates of produced electron-positron pairs. Thus, we compare both situations, that is, when one takes into account or disregards the nuclear recoil, for the total probability rates defined as

$$W = \sum_N W_N, \quad (44)$$

where  $W_N$  is the  $N$ -photon probability rate of pair production. In the case considered in this article, this is given by Eq. (37), while the summation in (44) is over all photons  $N$ . More information on the theory describing the situation when one disregards the nuclear recoil can be found in Ref. [38]. Additionally, in Ref. [38], we worked out the Monte Carlo method of estimating the sum over  $N$  and spatial integrals that arise in  $W_N$ . Let us note that in the present case, when the

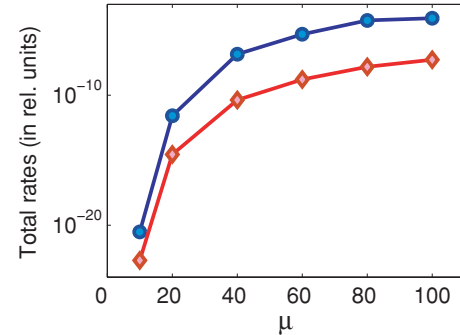


FIG. 14. (Color online) The total rates of electron-positron pair creation as a function of the dimensionless parameter  $\mu$  for the linearly polarized laser field ( $\delta = 0$ ) and for the laser frequency  $\omega = 0.01m_e c^2$ . The results are shown for  $\mu = 10, 20, 40, 60, 80$ , and  $100$ . The blue circles correspond to the case when the nuclear recoil is taken into account, while the red diamonds are for the case when one disregards the recoil effect. These points are connected by lines to guide the eye. A very pronounced enhancement (up to four orders of magnitude) is observed when a more accurate approach with an exact account for the nuclear recoil is applied.

differential probability rates are rapidly oscillating functions of the nuclear recoil, it is rather difficult to explicitly calculate the total rates. For this reason, we choose to estimate them using the same Monte Carlo method [38].

Figure 14 shows total probability rates for pair creation for the case of a linearly polarized laser field (with  $\delta = 0$ ) when its frequency is  $\omega = 0.01m_e c^2$  as a function of the dimensionless relativistic invariant parameter  $\mu$ . Here,  $\mu$  takes the values 10, 20, 40, 60, 80, and 100. The blue circles mark the results that are obtained using our more accurate approach of treating the colliding nucleus, that is, with the exact account for the nuclear recoil. These results were obtained assuming that the net number of photons exchanged between the nucleus and the laser field is zero,  $L = 0$  [see Eq. (28) for the definition of  $L$ ]. On the other hand, red diamonds correspond to the case when one disregards the recoil imparted on the nucleus, treating it as an infinitely heavy particle. In both cases, the presented rates (connected by lines to guide the eye) were calculated using more than  $10^9$  sample points. For the parameters considered here, a tremendous enhancement (up to four orders of magnitude) of the total probability rates of pair creation is observed when one takes into account the nuclear recoil. The reason for such a significant discrepancy between these two situations is that the number of absorbed laser photons is much smaller when the recoil is accounted for. The situation might be different, however, when only few laser photons are needed for the pair creation. This case is going to be considered elsewhere. In addition, one can see from Fig. 14 that with increasing the parameter  $\mu$  the total rates tend to saturate, which is the case for both situations.

## VI. CONCLUSIONS

In the present article, the results for electron-positron pair creation in the head-on laser-nucleus collisions that account for the nuclear recoil have been presented. While there is recent work by Müller and Müller [46], where the authors consider

pair creation by highly energetic photons (mainly the one-, two-, and three-photon pair creation), we have described here the multiphoton pair creation. In light of both these works, it is important to realize that the pair creation with zero nuclear recoil is energetically forbidden, which has been proved here from first principles.

Variations in triply differential probability rates for laser-induced electron-positron pair creation due to the nuclear recoil have been studied in this article in great detail. For instance, our analysis has shown a dramatic dependence of the corresponding probability rates on the polarization of the laser wave impinging on the nucleus, with the highest efficiency of pair production in the case of a linearly polarized laser field. Let us emphasize that such a dependence is characteristic only for multiphoton processes, not for few-photon processes [46]. Moreover, our results for different geometries have shown that for the linear polarization the respective probability rates significantly increase if the colliding nucleus is detected in the direction of the laser-field propagation. Thus, we have mainly focused on this situation.

We have demonstrated that the differential probability rates for electron-positron pair creation increase tremendously owing to the nuclear recoil. At the same time, the differential probability rates oscillate rapidly with varying the energy transfer from the nucleus, which is not observed for instance in the case of few-photon pair production [46]. These rapid interference oscillations make it rather difficult to calculate the total probability rate of pair production in the tunneling regime. We have estimated it by means of the Monte Carlo method and have compared it with the result for the corresponding case when one neglects the nuclear recoil. For the parameters considered in the article, we have found a tremendous increase in the total rate of pair production when one uses a more accurate approach for treating the colliding nucleus.

#### ACKNOWLEDGMENTS

We thank Fritz Ehlotzky for very inspiring discussions and interest in the present work. We thank Anthony F. Starace and Evgeny A. Pronin for their comments regarding presented results. This work is supported by the Polish Ministry of Science and Higher Education under Grant No. N N202 033337.

#### APPENDIX: SOLVING THE FOUR-MOMENTUM CONSERVATION CONDITION

In accordance with Eq. (41), we analyze here the solutions to the four-momentum conservation condition,

$$\bar{p} + \bar{q} + \bar{r} = 0, \quad (\text{A1})$$

where  $\bar{p}$  and  $\bar{q}$  are unknown laser-field-dressed momenta such that

$$\bar{p} = p + \frac{(e_p A_0)^2}{4(p \cdot n)} n, \quad (\text{A2})$$

$$\bar{q} = q + \frac{(e_q A_0)^2}{4(q \cdot n)} n, \quad (\text{A3})$$

which fulfill the on-mass-shell relations

$$\bar{p}^2 = (\bar{m}_p c)^2, \quad (\text{A4})$$

$$\bar{q}^2 = (\bar{m}_q c)^2. \quad (\text{A5})$$

Moreover, we assume that  $\bar{r}$  present in Eq. (A1) is known, but in principle it can be an arbitrary four-vector that does not satisfy an on-mass-shell relation. In the following, we keep the direction of the vector  $\mathbf{p}$  as known; we further denote it as  $\mathbf{n}_p$ . Expressing now  $\bar{q}$  in terms of  $\bar{p}$  and  $\bar{r}$ , which follows from Eq. (A1), we find out from Eq. (A5) that

$$\bar{r}^2 + 2(\bar{p} \cdot \bar{r}) + \bar{m}_p^2 c^2 - \bar{m}_q^2 c^2 = 0. \quad (\text{A6})$$

The preceding formula can be rewritten using Eq. (A2),

$$(p \cdot n)(p \cdot \bar{r}) + \kappa(p \cdot n) + \zeta = 0, \quad (\text{A7})$$

where we have introduced two constants  $\kappa$  and  $\zeta$ ,

$$\kappa = \frac{1}{2} (\bar{r}^2 + \bar{m}_p^2 c^2 - \bar{m}_q^2 c^2), \quad (\text{A8})$$

$$\zeta = \frac{(e_p A_0)^2}{4} (n \cdot \bar{r}). \quad (\text{A9})$$

Besides, let us recall that  $p = (E_p/c, \mathbf{p})$ ,  $n = (1, \mathbf{n})$ , and there is the dispersion relation  $E_p/c = \sqrt{\mathbf{p}^2 + m_p^2 c^2}$ . Let us also explicitly write down that  $\bar{r} = (\bar{r}_0, \bar{\mathbf{r}})$ . With this in mind, we can derive the following fourth-order equation to be satisfied by  $|\mathbf{p}|$ ,

$$\begin{aligned} & |\mathbf{p}|^4 [(\mathbf{n}_p \cdot \bar{\mathbf{r}})^2 + \bar{r}_0^2 (\mathbf{n}_p \cdot \mathbf{n})^2 - \bar{r}_0^2 - (\mathbf{n}_p \cdot \mathbf{n})^2 (\mathbf{n}_p \cdot \bar{\mathbf{r}})^2] \\ & + 2\kappa |\mathbf{p}|^3 (\mathbf{n}_p \cdot \bar{\mathbf{r}}) [(\mathbf{n}_p \cdot \mathbf{n})^2 - 1] + |\mathbf{p}|^2 \{ m_p^2 c^2 [(\mathbf{n}_p \cdot \bar{\mathbf{r}})^2 \\ & + \bar{r}_0^2 (\mathbf{n}_p \cdot \mathbf{n})^2 - 2\bar{r}_0^2] - \kappa^2 [(\mathbf{n}_p \cdot \mathbf{n})^2 - 1] \\ & - 2\zeta [\bar{r}_0 + (\mathbf{n}_p \cdot \mathbf{n})(\mathbf{n}_p \cdot \bar{\mathbf{r}})] \} + 2\kappa |\mathbf{p}| [\zeta (\mathbf{n}_p \cdot \mathbf{n}) \\ & - m_p^2 c^2 (\mathbf{n}_p \cdot \bar{\mathbf{r}})] + \kappa^2 m_p^2 c^2 - (\zeta + \bar{r}_0 m_p^2 c^2)^2 = 0. \end{aligned} \quad (\text{A10})$$

Solving this equation for the fixed direction  $\mathbf{n}_p$ , we are able to specify the momentum  $\mathbf{p}$ , and hence also the momentum  $\mathbf{q}$ . Among all four solutions of Eq. (A10),  $|\bar{\mathbf{p}}|^{(\ell)}$  where  $\ell = 1, 2, 3, 4$ , we choose only those which are real and positive and for which the zero component of  $\bar{\mathbf{q}}$  is also positive. In particular, for the analysis presented in this article we have

$$\bar{p} = \bar{p}_{e^-}, \quad \bar{q} = \bar{p}_{e^+}, \quad \bar{r} = \bar{q}_f - \bar{q}_i - Nk, \quad (\text{A11})$$

in the four-momentum conservation law (41). Let us also note that in the case of a zero-momentum transfer from the nucleus, when  $\bar{q}_f = \bar{q}_i$ , we have  $\kappa = 0$  and  $\zeta = 0$ , and so Eq. (A10) is simplified to the form

$$\begin{aligned} & |\mathbf{p}|^4 [(\mathbf{n}_p \cdot \mathbf{n})^2 - 1]^2 - 2|\mathbf{p}|^2 (m_p c)^2 \\ & \times [(\mathbf{n}_p \cdot \mathbf{n})^2 - 1] + (m_p c)^4 = 0. \end{aligned} \quad (\text{A12})$$

As follows from this equation, if only  $\mathbf{n}_p \cdot \mathbf{n} \neq 1$  there is a double root to this equation,

$$|\mathbf{p}|^2 = \frac{(m_p c)^2}{2[(\mathbf{n}_p \cdot \mathbf{n})^2 - 1]}, \quad (\text{A13})$$

which, however, is negative. In other words, the four-momentum conservation law given by Eq. (41) has no physical solutions if one neglects the nuclear recoil.

- [1] M. Marklund and P. Shukla, *Rev. Mod. Phys.* **78**, 591 (2006).
- [2] Y. I. Salamin, S. X. Hu, K. Z. Hatsagortsyan, and C. H. Keitel, *Phys. Rep.* **427**, 41 (2006).
- [3] F. Ehlotzky, K. Krajewska, and J. Z. Kamiński, *Rep. Prog. Phys.* **72**, 046401 (2009).
- [4] M. H. Thoma, *Rev. Mod. Phys.* **81**, 959 (2009).
- [5] C. Müller, A. B. Voitkiv, and B. Najjari, *J. Phys. B* **42**, 221001 (2009).
- [6] A. B. Voitkiv, B. Najjari, and J. Ullrich, *Phys. Rev. Lett.* **103**, 193201 (2009).
- [7] M. Boca and V. Florescu, *Phys. Rev. A* **80**, 053403 (2009); N. B. Narozhny and M. S. Fofanov, *Zh. Eksp. Teor. Fiz.* **110**, 26 (1996) [*JETP* **83**, 14 (1996)].
- [8] F. Sauter, *Z. Phys.* **69**, 742 (1931).
- [9] J. Schwinger, *Phys. Rev.* **82**, 664 (1951).
- [10] E. Brezin and C. Itzykson, *Phys. Rev. D* **2**, 1191 (1970).
- [11] V. S. Popov, *Zh. Eksp. Teor. Fiz.* **61**, 1334 (1971) [*Sov. Phys. JETP* **34**, 709 (1972)].
- [12] G. A. Mourou, T. Tajima, and S. V. Bulanov, *Rev. Mod. Phys.* **78**, 309 (2006).
- [13] V. Yanovsky, V. Chvykov, G. Kalinchenko, P. Rousseau, T. Planchon, T. Matsuoka, A. Maksimchuk, J. Nees, G. Cheriaux, and K. Krushelnick, *Opt. Express* **16**, 2109 (2008).
- [14] See the online proposal at [<http://www.extreme-light-infrastructure.eu>].
- [15] M. Altarelli *et al.*, Technical Design Report of the European XFEL, DESY 2006-097, available online at [<http://www.xfel.eu>].
- [16] L. F. DiMauro, J. Arthur, N. Berrah, J. Bozek, J. N. Galayda, and J. Hastings, *J. Phys. Conf. Ser.* **88**, 012058 (2007).
- [17] H. R. Reiss, *J. Math. Phys.* **3**, 59 (1962).
- [18] L. S. Brown and T. W. B. Kibble, *Phys. Rev. A* **133**, 705 (1964).
- [19] A. I. Nikishov and V. I. Ritus, *Zh. Eksp. Teor. Fiz.* **46**, 776 (1964) [*Sov. Phys. JETP* **19**, 529 (1964)].
- [20] N. B. Narozhny, A. I. Nikishov, and V. I. Ritus, *Zh. Eksp. Teor. Fiz.* **47**, 930 (1964) [*Sov. Phys. JETP* **20**, 622 (1965)].
- [21] N. B. Narozhny and M. S. Fofanov, *Laser Phys.* **7**, 141 (1997).
- [22] V. S. Popov, *Pis'ma Zh. Eksp. Teor. Fiz.* **74**, 151 (2001) [*JETP Lett.* **74**, 133 (2001)].
- [23] A. Ringwald, *Phys. Lett. B* **510**, 107 (2001).
- [24] H. K. Avetissian, A. K. Avetissian, G. F. Mkrtchian, and K. V. Sedrakian, *Phys. Rev. E* **66**, 016502 (2002).
- [25] A. Di Piazza, *Phys. Rev. D* **70**, 053013 (2004).
- [26] D. B. Blaschke, A. V. Prozorkevich, C. D. Roberts, S. M. Schmidt, and S. A. Smolyansky, *Phys. Rev. Lett.* **96**, 140402 (2006).
- [27] A. R. Bell and J. G. Kirk, *Phys. Rev. Lett.* **101**, 200403 (2008).
- [28] V. P. Yakovlev, *Zh. Eksp. Teor. Fiz.* **49**, 318 (1965) [*Sov. Phys. JETP* **22**, 223 (1996)].
- [29] M. H. Mittleman, *Phys. Rev. A* **35**, 4624 (1987).
- [30] E. P. Liang, S. C. Wilks, and M. Tabak, *Phys. Rev. Lett.* **81**, 4887 (1998).
- [31] K. Dietz and M. Pröbsting, *J. Phys. B* **31**, L409 (1998).
- [32] H. K. Avetissian, A. K. Avetissian, G. F. Mkrtchian, and Kh. V. Sedrakian, *Nucl. Instrum. Methods Phys. Res. A* **507**, 582 (2003).
- [33] C. Müller, A. B. Voitkiv, and N. Grün, *Nucl. Instrum. Methods Phys. Res. B* **205**, 306 (2003).
- [34] C. Müller, A. B. Voitkiv, and N. Grün, *Phys. Rev. A* **67**, 063407 (2003).
- [35] C. Müller, A. B. Voitkiv, and N. Grün, *Phys. Rev. Lett.* **91**, 223601 (2003).
- [36] C. Müller, A. B. Voitkiv, and N. Grün, *Phys. Rev. A* **70**, 023412 (2004).
- [37] P. Sieczka, K. Krajewska, J. Z. Kamiński, P. Panek, and F. Ehlotzky, *Phys. Rev. A* **73**, 053409 (2006).
- [38] J. Z. Kamiński, K. Krajewska, and F. Ehlotzky, *Phys. Rev. A* **74**, 033402 (2006).
- [39] K. Krajewska, J. Z. Kamiński, and F. Ehlotzky, *Laser Phys.* **16**, 272 (2006).
- [40] A. I. Milstein, C. Müller, K. Z. Hatsagortsyan, U. D. Jentschura, and C. H. Keitel, *Phys. Rev. A* **73**, 062106 (2006).
- [41] M. Yu. Kuchiev and D. J. Robinson, *Phys. Rev. A* **76**, 012107 (2007).
- [42] K. Krajewska and J. Z. Kamiński, *Laser Phys.* **18**, 185 (2008).
- [43] C. Deneke and C. Müller, *Phys. Rev. A* **78**, 033431 (2008).
- [44] C. Müller, *Phys. Lett. B* **672**, 56 (2009).
- [45] E. Lötstedt, U. D. Jentschura, and C. H. Keitel, *New J. Phys.* **11**, 013054 (2009).
- [46] S. J. Müller and C. Müller, *Phys. Rev. D* **80**, 053014 (2009).
- [47] D. M. Volkov, *Z. Phys.* **94**, 250 (1935).
- [48] L. V. Keldysh, *Zh. Eksp. Teor. Fiz.* **47**, 1945 (1964) [*Sov. Phys. JETP* **20**, 1307 (1965)].
- [49] A. M. Perelomov, V. S. Popov, and M. V. Terent'ev, *Zh. Eksp. Teor. Fiz.* **50**, 1393 (1966) [*Sov. Phys. JETP* **23**, 924 (1966)].
- [50] F. H. M. Faisal, *J. Phys. B* **6**, L89 (1973).
- [51] H. R. Reiss, *Phys. Rev. A* **22**, 1786 (1980).
- [52] D. J. Griffiths, *Introduction to Electrodynamics* (Prentice-Hall, Englewood Cliffs, NJ, 1999).
- [53] D. L. Burke *et al.*, *Phys. Rev. Lett.* **79**, 1626 (1997).
- [54] C. Bamber *et al.*, *Phys. Rev. D* **60**, 092004 (1999).
- [55] See [<http://www.attoworld.de>].
- [56] C. Itzykson and J.-B. Zuber, *Quantum Field Theory* (McGraw-Hill, New York, 1980).
- [57] W. Becker, A. Lohr, and M. Kleber, *J. Phys. B* **27**, L325 (1994).
- [58] K. J. Schafer, B. Yang, L. F. DiMauro, and K. C. Kulander, *Phys. Rev. Lett.* **70**, 1599 (1993).
- [59] B. Borca, M. V. Frolov, N. L. Manakov, and A. F. Starace, *Phys. Rev. Lett.* **88**, 193001 (2002).
- [60] K. Krajewska, I. I. Fabrikant, and A. F. Starace, *Phys. Rev. A* **74**, 053407 (2006).
- [61] N. L. Manakov and M. V. Frolov, *Pis'ma Zh. Eksp. Teor. Fiz.* **83**, 630 (2006) [*JETP Lett.* **83**, 536 (2006)].
- [62] K. Krajewska, I. I. Fabrikant, and A. F. Starace, *Laser Phys.* **17**, 368 (2007).
- [63] K. Krajewska, I. I. Fabrikant, and A. F. Starace, *Phys. Rev. A* **78**, 023407 (2008).